

High-resolution offshore wind resource assessment at turbine hub height with Sentinel-1 SAR data and machine learning

Louis de Montera¹, Henrick Berger¹, Romain Husson¹, Pascal Appelghem², Laurent Guerlou¹, Mauricio Fragoso¹

¹CLS Collecte Localisation Satellites, Ramonville-Saint-Agne, France

²Atmosky, Talence, France

Correspondence to: Romain Husson (rhusson@groupcls.com)

Abstract. This paper presents a method to calculate offshore wind power at turbine hub height from Sentinel-1 Synthetic Aperture Radar (SAR) data using machine learning. The method is tested in two 70 km x 70 km areas off the Dutch coast where ~~measurements from Doppler wind Lidars installed at the sea surface measurements from commercial instruments deployed for offshore wind energy site investigations~~ Lidar measurements are available and can be used as a reference. Firstly, SAR wind ~~speeds~~ at surface level are improved with a machine learning algorithm using geometrical characteristics of the sensors and parameters related to the atmospheric stability extracted from a high-resolution numerical model. The SAR wind speed bias ~~against Lidar measurements~~ at 10 m above sea level is reduced from -0.42 m s^{-1} to 0.02 m s^{-1} , and its ~~standard deviation~~ RMSE standard deviation from 1.41 m s^{-1} to 0.98 m s^{-1} . After improvement, SAR surface wind ~~speeds~~ are extrapolated at higher altitudes with a separate machine learning algorithm trained with the wind profiles measured by the Lidars and additional parameters from the high-resolution numerical model. ~~We show that, if profiling Lidars are available in the area of study, these two steps can be combined into a single one, in which the machine learning algorithm is trained directly at turbine hub height.~~ Once the wind speed at turbine hub height is obtained, ~~we assume the presence of an 810 MW turbine with a simplified typical power curve. The~~ extractable wind power is ~~calculated by obtaining the wind speed Weibull distribution using with the method of the moments, and to obtain the wind speed Weibull distribution, which is then and then multiplying it multiplied by the turbine power curve. The results are given assuming an 8 MW turbine typical power curve.~~ The accuracy of the ~~extractible~~ wind power derived from SAR data ~~when compared with Lidar measurements is $\pm 3-4\%$ when compared with Lidars.~~ The additional error due to SAR satellites low temporal ~~sampling is estimated at $\pm 2\%$, but this error can be easily removed by using a numerical model to simulate the satellites' passages and estimating it for this typical turbine.~~ ~~Then~~ Finally, wind power maps at 200 m are presented and compared with the ~~raw~~ outputs of the numerical model at the same altitude. The maps based on SAR data have a much ~~better~~ higher level of details, ~~in particular regarding especially for~~ the coastal wind gradient. The new revealed patterns show differences with the numerical ~~model~~ of as much as 10% in some locations ~~over distances of the order of 20 km~~. We conclude that SAR data

combined with a high-resolution numerical model and machine learning techniques can improve the wind power estimation at turbine hub height, and thus provide useful insights for optimizing wind farm siting and risk management.

35 1 Introduction

Estimating the ~~available-extractible~~ offshore wind power at turbine hub height is a challenging problem due to the difficulty in measuring the wind profile in the boundary layer over the sea. Currently, ~~two main methods are used to estimate the offshore extractible power at hub height: is estimated by using~~ numerical models and/or ~~Doppler wind floating~~-Lidars ~~installed at the sea surface pointing upwards~~ (NREL, 2020). ~~Floating~~-Lidars provide ~~direct measurements of~~ the complete wind profile at one
40 location with a high temporal sampling, but ~~they~~ are very expensive to operate. Therefore, only one or two are typically used to sound large areas. Conversely, numerical models provide outputs over the entire area of interest. ~~However, they are not capable of resolving small scale phenomena due to their physics and resolution. As a result, their errors are not precisely known and may vary in time and space. This is particularly relevant~~ problematic in coastal areas where processes are more complex and where the wind gradient is strong ~~involve smaller scales.~~

~~but they tend to flatten heterogeneities and extremes. Moreover, their errors are not precisely known, primarily because of the lack of representation of sub-grid processes. As a result~~ Due to these limitations, considerable uncertainty remains about actual offshore wind resources, which can affect wind farm project planning and management. ~~This is particularly relevant in coastal areas where processes are more complex and where the wind gradient is strong.~~

The need to improve wind speed assessment, and thus estimating more precisely wind power availability throughout wind
50 farms' life cycle, has led to a growing interest in using ~~remote sensing~~ satellite data to estimate wind resources (see, e.g., Hasager et al., 2015). Contrary to ~~ground-based~~ Lidars, spaceborne sensors have the advantage of sounding large areas with high spatial resolution. However, they are not perfect: their revisit period is typically ~~low-long~~ (a couple of days for Sentinel-1 in Europe, for example); and they use ~~an indirect measurement~~ measurement based on ~~by estimating the offshore surface wind from~~ the sea state ~~Radar backscatter~~. Therefore, their measurements are impacted by several sources of potential error
55 (~~low temporal sampling~~, sensor geometry, currents, algae, bright targets, ~~rain cells~~, bathymetry, turbulence, etc.). Moreover, the extrapolation of their measurements ~~from the sea surface~~ to hub height is not an easy task due to the variety of meteorological conditions ~~that may impact the wind speed extrapolation ratio.~~

Several studies have ~~already~~ attempted to assess offshore wind power potential with spaceborne scatterometers, such as ERS-1, ERS-2, NSCAT, QuickSCAT, and ASCAT (Sánchez et al., 2007; Pimenta et al., 2008; Karagali et al., 2014; Bentamy and
60 Croize-Fillon, 2014; Remmers et al., 2019). However, the resolution of these instruments is at best 12.5 km², which is not adapted to coastal areas due to land contamination. ~~In this context~~, Synthetic Aperture Radar (SAR) satellites are an interesting alternative because wind products derived from their measurements have a much finer resolution of 1 km. The potential of

SAR data has already been assessed by numerous studies (Hasager et al., 2002; Hasager et al., 2005; Hasager et al., 2006; Christiansen et al., 2006; Hasager et al., 2011; Hasager et al., 2014; Chang et al., 2014; Chang et al., 2015; Hasager et al., 2020). However, validating SAR measurements with in-situ data has been limited (Ahsbahs et al., 2017; Badger et al., 2019; de Montera et al., 2020; Ahsbahs et al., 2020) and these studies concluded that important biases remained. (in the context of this study, the term ‘in-situ instruments’ includes profiling Lidars, although technically they use remote sensing). Therefore, more research is needed to improve the estimation of wind resources at hub height with SAR data and convince the industry to use them.

~~Regarding Concerning~~ the extrapolation of the surface wind speeds to higher altitudes, interesting methods have been proposed in the literature based on power laws or the statistical theory of turbulence (Grachev and Fairall, 1996; Hsu et al., 1994; Badger et al., 2016); however, the problem has not been satisfactorily resolved and becomes increasingly critical as the typical height of windmills increases. Therefore, more research is needed to improve the estimation of wind resources at hub height with SAR data and convince the industry to use them. The extrapolation of surface wind speeds to higher altitudes is a challenging problem given the diversity of meteorological conditions and the variability of turbulence intensity in the boundary layer. ~~The statistical theory of turbulence provides theoretical wind profiles (see, e.g., Grachev and Fairall, 1996).~~ However, the problem has not been satisfactorily resolved and becomes increasingly critical as the typical height of windmills increases. Empirical evidence Data analysis from offshore meteorological masts measurements suggests that a simple power law could be sufficient to model the wind profile (Hsu et al., 1994). However Nevertheless, the analysis of our Lidar data shows that, above 40 m, this power law model is no longer accurate. This limitation has led some authors to use numerical models to improve the extrapolation to higher altitudes (Badger et al., 2016). The advantage of numerical models is that they provide information about atmospheric stability through parameters like surface temperature and surface heat flux. In Badger et al. (2016), these surface parameters were averaged and combined with the similarity theory of Monin-Obukhov to extrapolate wind Weibull parameters. However, to our knowledge, this method was validated with only one meteorological mast in the Baltic Sea and not higher than an altitude of 100 m. Therefore, more research is needed to improve the estimation of wind resources at hub height at hub height with SAR data, and convince the industry to use them. Moreover, Optis et al. (2021) found that using machine learning was more efficient than using a theoretical approach.

~~In this study, we propose a method to overcome these limitations by using machine learning. Given Due the complexity of the relation between wind speed and the sea state and to the high number of possible sources of error in the retrieval of surface winds with SAR satellites, machine learning seemss appropriate to improve the accuracy of retrieval of surface wind speeds with SAR- surface wind speedssatellites. Regarding their extrapolation at higher altitudes, on land, machine learning has also been found to improve the accuracy of the wind speeds extrapolated at turbine hub height compared to classical extrapolation methods based on power laws or logarithmic laws (Türkan et al., 2016; Mohandes and Rehman, 2018; Vassallo et al., 2019). Moreover, Optis et al. (2021) also found that machine learning was more efficient at extrapolating offshore winds than theoretical approaches. Moreover, it has also been shown that, even if the algorithm is trained with a few in-situ instruments,~~

it can be applied in a large area around them without significantly degrading the accuracy (Bodini and Optis, 2020; Optis et al., 2021). Moreover, Optis et al. (2021) found that machine learning was more efficient at extrapolating offshore winds than theoretical approaches. Therefore, we also chose to use machine learning in order to derive the wind speeds at hub height based on the SAR surface winds. As in Badger et al. (2016), we take advantage of a numerical model to assess the atmospheric stability and provide the algorithm with the relevant meteorological parameters and by combining SAR data with a numerical model. On land, machine learning has been found to give good results compared to classical extrapolation methods based on power laws or logarithmic laws (Türkan et al., 2016; Mohandes and Rehman, 2018; Vassallo et al., 2019). It has also been shown that, even if the algorithm is trained with a few in-situ instruments, it can be applied in a large area around them without significantly degrading the accuracy (Bodini and Optis, 2020; Optis et al., 2021).

Section 2 describes the numerical model, the SAR data used in this study (Sentinel-1 constellation satellites), the numerical model, the Lidar data used as a reference to train the algorithms, and the formulas used to compute the wind power. Section 3 describes the two machine learning algorithms designed to improve the accuracy of SAR surface winds and the second machine learning algorithm used to extrapolate the surface winds to hub height, respectively. In this paper, we use SAR data from Sentinel-1 A and B satellites that provide the surface wind over the sea and improve them with the random forest algorithm. The reason for separating the method into two steps algorithms is that it is the scarcity of offshore Lidar data. Since the first algorithm improvement of correcting SAR surface wind biases utilizes depends on geometric properties of the sensor, it may be improved by using a large network of classical metocean buoys as a training dataset in the future that are specific to the location. On the contrary, the algorithm extrapolating the surface winds to higher altitudes only depends on meteorological parameters related to the atmospheric stability. Therefore, it can be trained with a few Lidars in one location data obtained in one place and applied in other areas (if similar meteorological conditions are met), which is necessary given the scarcity of Lidar data. First, a method is proposed to deal with the case where only surface in-situ measurements are available. In that case, the method requires two separate random forest algorithms: the first one improves SAR winds at surface level and the second one extrapolates them at turbine hub height. The reason for separating the method into two steps is that the improvement of SAR winds utilizes geometric properties of the sensor that are specific to the location. On the contrary, the algorithm extrapolating the surface wind to higher altitudes only depends on parameters related to the atmospheric stability. It can therefore be trained with Lidar data as a reference and applied in other areas. In the case where profiling Lidars are available in the study area study, these two algorithms can be combined into a single algorithm trained directly at hub height. In Section 4, Both methods are the method is tested in two areas off the Dutch coast where profiling Lidar data are available.

The SAR wind speeds extrapolated at hub height are converted into a Weibull distribution, and the extractible power is obtained by simulating the presence of a typical 8-10 MW wind turbine operating at 200 m. The resulting maps are presented and compared with the output of the numerical model in order to estimate the benefit of using these methods compared with a state-of-the-art technique.

2 Data and Methodology

130 2.1 High-resolution numerical model

The two zones of study are located off the Dutch coast ~~and presented in~~ (Figure 1). They have an approximate size of 70 x 70 km. Their geographic extent was defined in order to include ~~some~~-offshore profiling Lidars and a part of the coastline in order to ~~observe~~-observe the wind gradient. The WRF (Weather Research and Forecasting) ~~Nonnon-Hydrostatic-hydrostatic Mesomeso-scale Mmodel-developed~~ (Skamarock et al., 2019) by NOAA (National Oceanic and Atmospheric Administration)

135 was run over these areas with a resolution of 1 km. The Planetary Boundary Layer (PBL) parametrization of the model was based on Hahmann et al., 2020. It was fueled-forced at its boundary limits by a larger-scale model, the reanalyzed GFS (Global Forecast System) having a resolution of 0.5° developed by NCEP (National Centers for Environmental Prediction). This larger-scale model was downscaled before using it to force the WRF model. This type of numerical model is representative of how

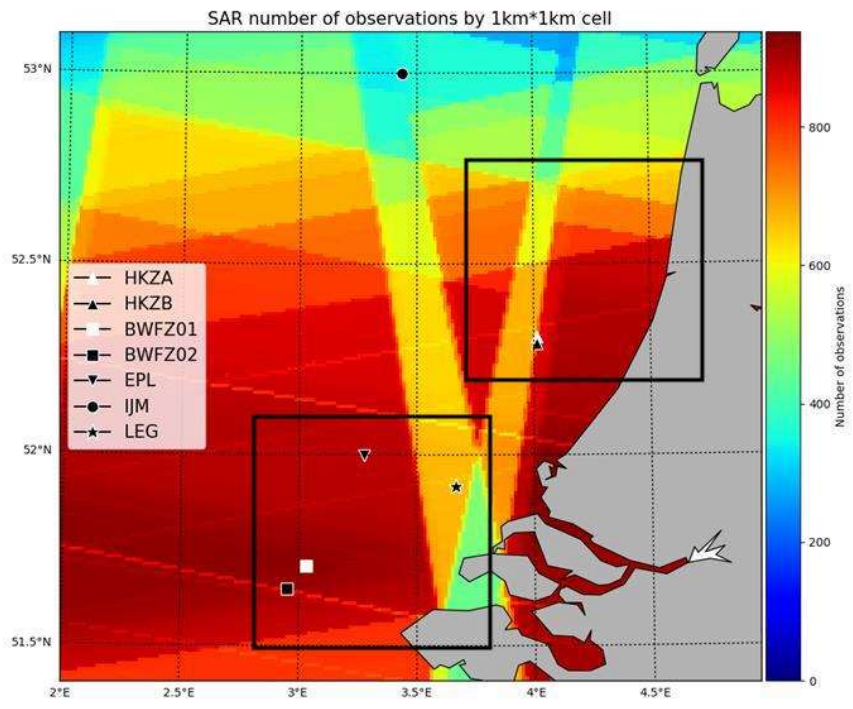
wind resources are currently assessed by the industry. Here, it is used to estimate the atmospheric stability and extrapolate

140 SAR ~~data-surface winds~~ to turbine hub height. ~~It was fueled at its boundary limits by a larger-scale model, the reanalyzed GFS (Global Forecast System) having a resolution of 0.5° developed by NCEP (National Centers for Environmental Prediction). This larger-scale model was downscaled before using it to force the WRF model.~~ The WRF model was run over a period from

January ~~2015-2017~~ to ~~May-December~~ 2019~~20~~. It provides the wind speed and direction from ~~the~~-surface ~~and-up~~ to 200 m,

~~in~~with increments of 20 m. It also provides other meteorological variables, such as air and sea surface temperature, surface

145 heat flux, relative humidity, and pressure.



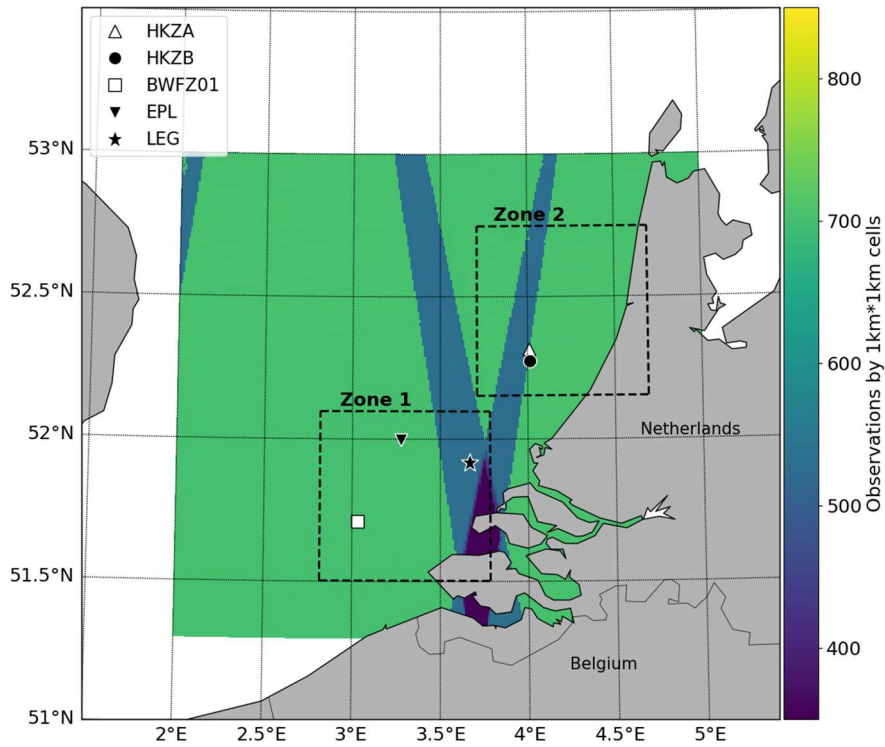


Figure 1: Locations of Zone 1 (bottom, latitude 51.50°N - 52.09°N / longitude 2.82°E - 3.77°E) and Zone 2 (top, latitude 52.15°N - 52.74°N / longitude 3.71°E - 4.68°E) with the positions of the profiling Lidars. The colour represents the number of Sentinel-1 SAR Level 2 wind observations during years 2017, 2018 and 2019. floating Lidars and total number of Sentinel-1 SAR L2 wind observations during years 2017, 2018 and 2019. The black boxes represent Zone 1 (bottom, latitude 51.50° - 52.09° / longitude 2.82° - 3.77°) and Zone 2 (top, latitude 52.15° - 52.74° / longitude 3.71° - 4.68°).

2.2 In-situ instruments

The dataset used in this study comprises five ground-based floating-profiling Lidars located off the Dutch coast (Figure 1). They are named HKZA, HKZB, BWFZ01, EPL and LEG. HKZ stand for Hollandse Kust Zuid wind farm, BWF for Borssele Wind Farm Zone, EPL for European Platform, and LEG for Lichteiland Goeree platform. Zone 1 includes the Lidars BWFZ01, EPL and LEG, and Zone 2 includes the Lidars HKZA and HKZB. Lidars HKZA, HKZB, BWFZ01 are floating. Lidars EPL and LEG are installed on platforms. The wind speed and direction are 10-minutes averaged around the observation times. The data were quality checked by our data provider C2WIND (for each time intervals, the minimum number of packets was set at 20 and the minimum availability at 80%). The wind speed and direction are 10-minutes averaged around the observation times. There are 7 Lidars in the dataset, respectively named HKZA, HKZB, BWFZ01, BWFZ02, EPL, LEG and IJM. HKZ stand for Hollandse Kust Zuid, BWF for Borssele Wind Farm Zone, EPL for European Platform, and LEG for Lichteiland

Goeree platform. Zone 1 includes the Lidars BWFZ01, EPL and LEG, and Zone 2 includes the Lidars HKZA and HKZB. Lidars HKZA, HKZB, BWFZ01 are floating and Lidars EPL and LEG are installed on platforms. The vertical sampling and the duration of these Lidar measurements varies between observation campaigns and are displayed in Table 1. Zone 1 includes the Lidars BWFZ01, BWFZ02, EPL and LEG, and Zone 2 includes the Lidars HKZA and HKZB. The IJM lidar provides a very long period of measurements, but unfortunately it stopped operating before the availability of the Sentinel 1 B data, and therefore was not used. Similarly, the Lidar BWFZ02 was functioning only for 4 months and its small quantity of data was found to be unreliable.

170

Lidar	Longitude	Latitude	First date	Last date	Number of levels	First-Lowest altitude	Last Highest altitude
HKZA	4.011°E	52.309°N	2016-06-05	2018-06-05	11	30m	200m
HKZB	4.013°E	52.292°N	2016-06-05	2018-06-05	11	30m	200m
LEG	3.667°E	51.917°N	2014-11-17	2017-03-31	10	61m	300m
EPL	3.276°E	51.998°N	2016-05-30	2017-03-31	11	61m	290m
IJM	3.436°E	52.998°N	2011-11-02	2016-03-09	14	26m	314m
BWFZ01	3.033°E	51.71°N	2015-06-11	2017-02-27	10	30m	200m
BWFZ02	2.952°E	51.65°N	2016-02-12	2016-06-22	10	30m	200m

175 Table 1: Main characteristics of the 7-five floating-profiling lidars

For each Lidar, the wind measured at the first altitude level is used to estimate the surface wind below at 10 m above sea level (a.s.l.), which is the altitude of SAR data. The extrapolation to 10 m a.s.l. is performed using a classical power law:

180

$$U_{10} = U_{min} \cdot \left(\frac{10}{Z_{min}} \right)^\alpha \quad \text{Eq. (1)}$$

where U_{10} is the wind speed at 10 m in m s^{-1} , U_{min} the Lidar wind speed at the first altitude level in m s^{-1} , and Z_{min} the altitude of the first level in m, and α a non-dimensional exponent. Hsu et al. (1994) recommend choosing an exponent of 0.11 over the

185 sea. We checked this hypothesis with HKZA and HKZB Lidars that were equipped with anemometers measuring wind speed
at 4 m a.s.l.. This ~~power law~~exponent was found to be ~~indeed correct on average~~correct on averageunbiased. However, in order
to refine the wind speed values ~~extrapolated~~ at 10 m a.s.l., we adapted ~~this~~the exponent depending on the current atmospheric
stability. The ~~empirical-instantaneous~~ exponents obtained with HKZA and HKZB Lidars were compared with the air-sea
190 temperature difference provided by the high-resolution numerical model WRF. The relation was fitted with a second-degree
polynomial (Figure 2) and ~~then the adaptive exponents were~~ used to obtain the wind speed at 10 m a.s.l.. The anemometers
located at the base of the Lidars at 4 m a.s.l. do not have a high precision and may add some uncertainty, however, since the
final machine learning algorithm presented in this study is trained with Lidar measurements at hub height, this uncertainty is
included in our results.

195

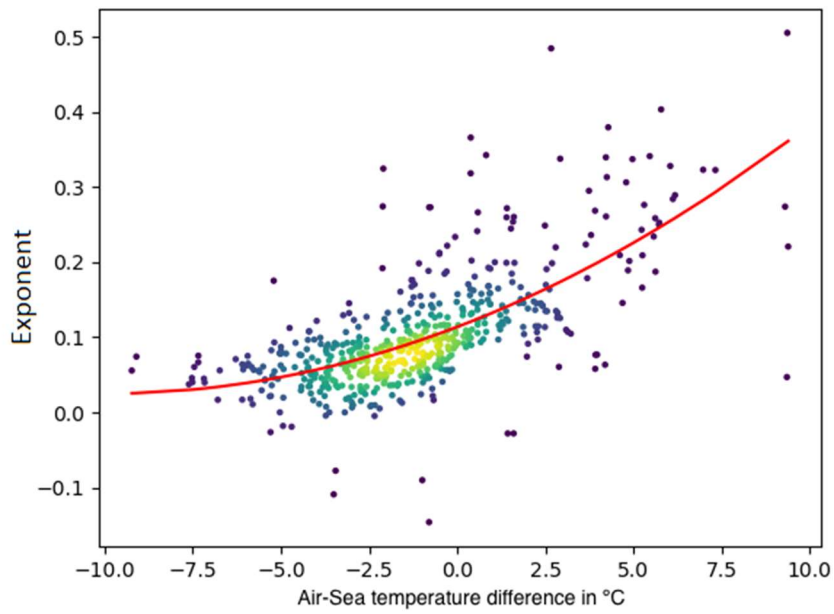
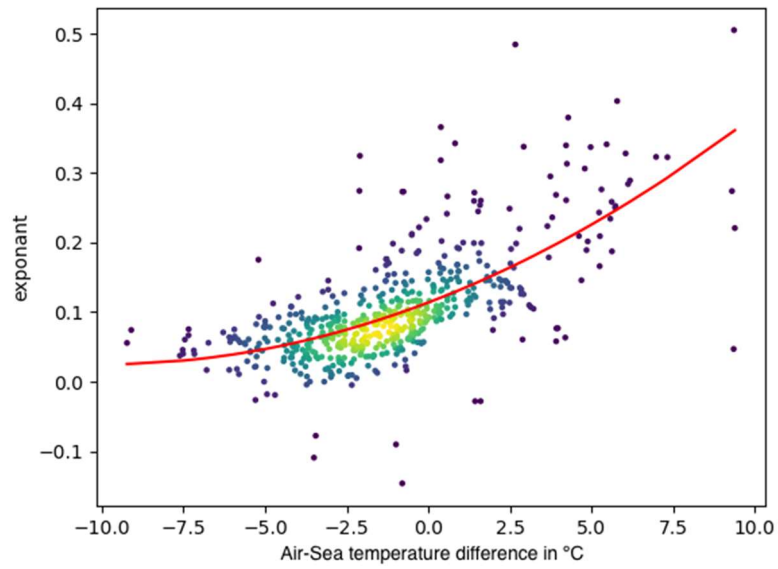


Figure 2: Exponent of the power law between the wind speeds at 4 m and 40 m as a function of the air-sea temperature difference fitted with a second-degree polynomial fit (red curve) with the following coefficients:- $Y= 0.1137 + 0.0178 X + 0.001 X^2$. The colours represent the density of points.

200

2.3 Sentinel-1 SAR data

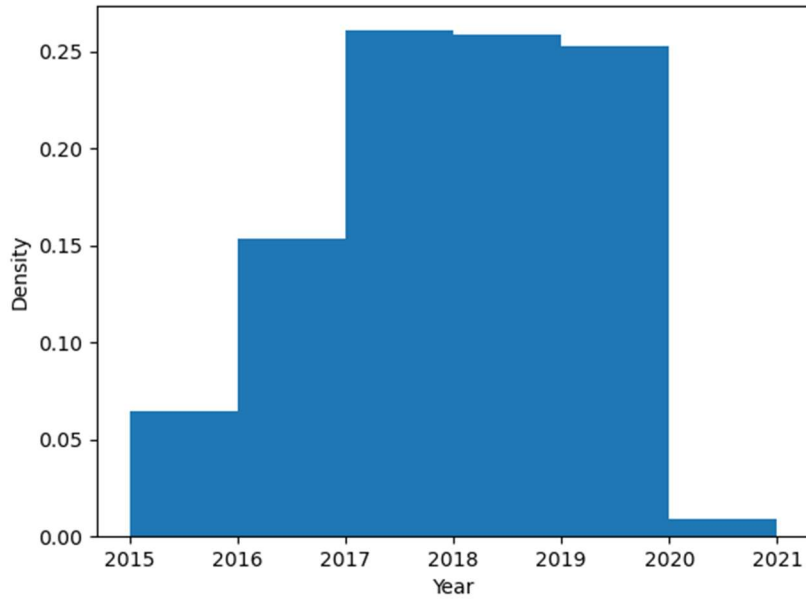
Sentinel-1 A and B are two polar-orbiting satellites equipped with C-band SAR. This sensor, which records surface roughness, has the advantage of operating day and night at wavelengths not impeded by cloud cover. The Sentinel-1 Level 1 GRD (Ground Range Detected) product has a grid spacing of a few tens of meters, whereas the Level 2 wind products typically have a resolution of 1 km. The two satellites are located on the same orbit 180° apart and at an altitude close to 700 km. In Dutch coastal waters, the acquisition mode is an Interferometric Wide (IW) swath using the TOPSAR technique, which provides a better-quality product by enhancing the image homogeneity (De Zan and Guarnieri, 2006). ~~All Sentinel-1 A and B SAR images in IW acquisition mode from 2014 to 2020 in the study areas were collected. The revisit rate is one passage every two days, which occurs usually in the morning around 5 AM or in the evening around 5 PM (UTC). The satellites pass in the morning or in the evening depending on the orbit orientation, descending or ascending, respectively. The exact acquisition time can vary by plus or minus 30 mn depending on the incidence angle under which the region of interest is observed. The constellation was only fully operational at the end of 2016. We collected a~~All Sentinel-1 A and B SAR images in IW acquisition mode ~~from for 2014 to 2020 in the study areas were collected. 2017, 2018 and 2019 only to ensure a complete and homogenous annual~~ ~~sampling. The total number of samples over these three years for the areas of interest is shown in Figure 1, on which shows it can be seen~~ that the coverage is not spatially uniform.

The Level 1 images were calibrated and corrected from the instrument noise provided as metadata. A dedicated bright target filtering was applied to remove Radar echoes created by ships, wind farms and other structures at sea. An additional filter (Koch, 2004) was used to identify heterogeneous signatures not related to wind, like currents, Radar interferences, and remaining bright targets. However, this filter has an increased sensitivity at low wind speeds, therefore, the identified pixels were not removed to avoid disrupting the wind speed Weibull distribution, which is necessary to estimate wind power. The information provided by this filter was only used to create maps of areas where wind power estimates are unreliable, typically due to dense regions of wind turbines or mooring areas, which are well identified on average by the heterogeneity filtering. Then, Level 1 SAR products were degraded to a 1 km resolution and Level-2 surface winds at 10 m a.s.l. were obtained using a Bayesian inversion scheme using as inputs the wind speed obtained by inverting the SAR backscatter with the CMOD5.N ~~Geophysical Model Function (GMF)geophysical model function~~ (KNMI, 2008; ECMWF, 2008; Hersbach, 2010) and the outputs of ECMWF (European Centre for Medium-Range Weather Forecasts) NWP (Numerical Weather Prediction) model to constrain the wind direction. The Level 2 product tiles were combined into a gridded map over the areas of interest, in order to form a data cube where each pixel corresponds to a time series of SAR measurements.

~~The revisit rate is one passage every two days, which occurs usually in the morning around 5 AM or in the evening around 5 PM (UTC). However, Figure 3, which gives the number of passages per year, shows that the constellation was only fully operational at the end of 2016. Therefore, we used SAR data from 2017, 2018 and 2019 when estimating the wind power to~~

ensure a complete and homogenous annual sampling. Figures 4 and 5 show the number of samples over these three years for each of the areas of interest.

235



~~Figure 3: Histogram of the number of SAR samples at Lidar HKZA's location. Before 2017, the constellation was not fully operational. In 2020, only two months of data had been collected at the time of this study. Therefore, only 2017, 2018 and 2019 are complete with regular passes.~~

240

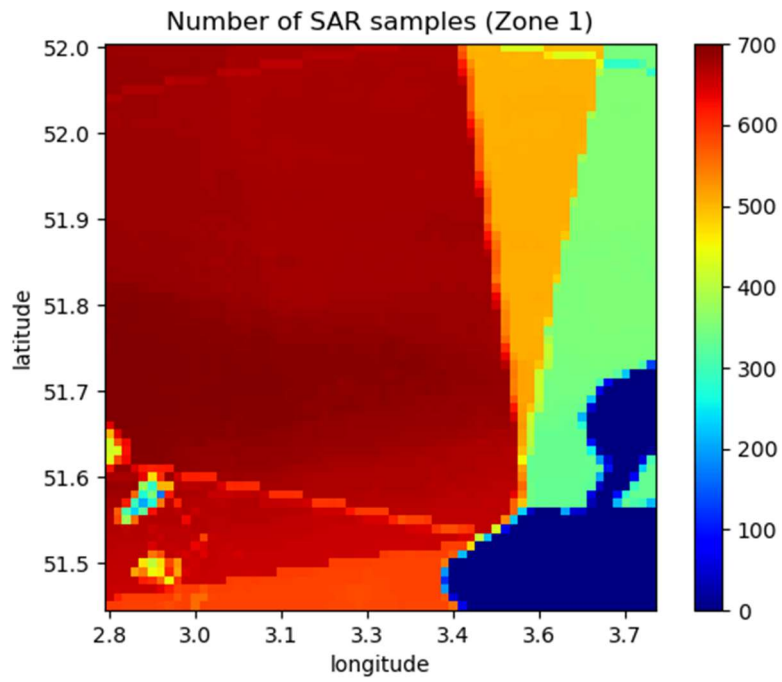


Figure 4: Number of Sentinel-1 SAR wind samples available over Zone 1 during 2017, 2018 and 2019.

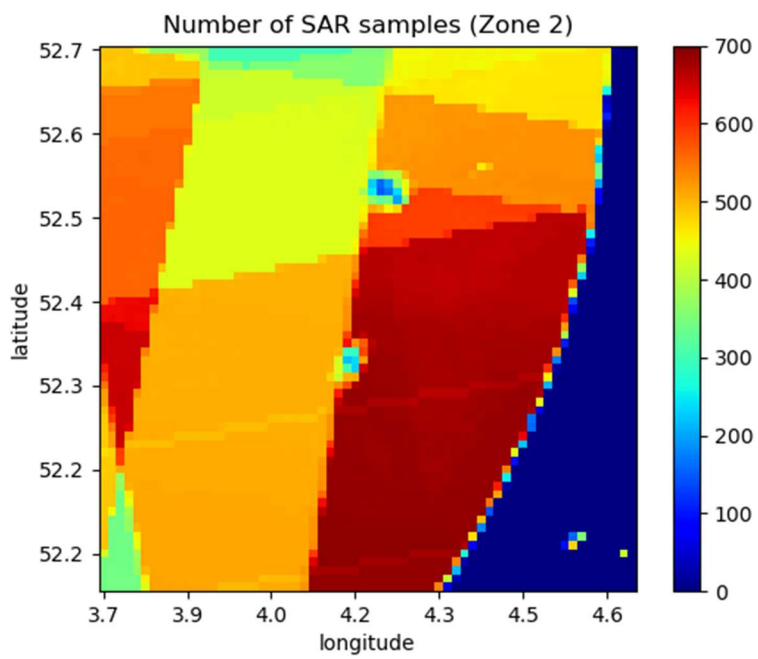


Figure 5: Number of Sentinel-1 SAR wind samples available over Zone 2 in 2017, 2018 and 2019.

2.4 Wind power estimation

The average extractible wind power P , hereafter simply called wind power, is calculated by multiplying point-by-point the wind speed probability density function (pdf) by the power curve of a specific wind turbine, ~~and then averaging the result~~. We chose to simulate an ~~8MW-10MW~~ turbine with a ~~simplified-typical~~ power curve: the DTU 10 MW Reference Wind Turbine V1 (see DTU Wind Energy, 2017, and https://github.com/NREL/turbine-models/blob/master/Offshore/DTU_10MW_178_RWT_v1.csv, last accessed September 2, 2021): ~~0 MW until a cut-in speed of 4 m s⁻¹, a linear increase until its nominal output at 15 m s⁻¹, then a plateau at 8MW until 25 m s⁻¹, and a storm mode for higher values during which the turbine stops to protect itself~~. A simple histogram could be used to estimate the wind speed pdf. However, due to the low number of SAR samples, a more efficient technique consists in using the SAR data to fit a Weibull pdf, which usually describes the wind speed accurately. The Weibull pdf is given by:

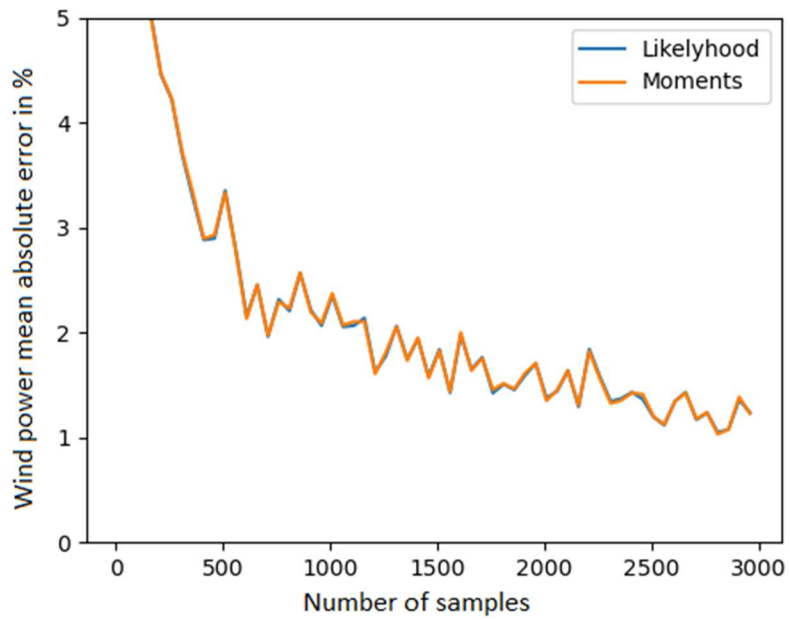
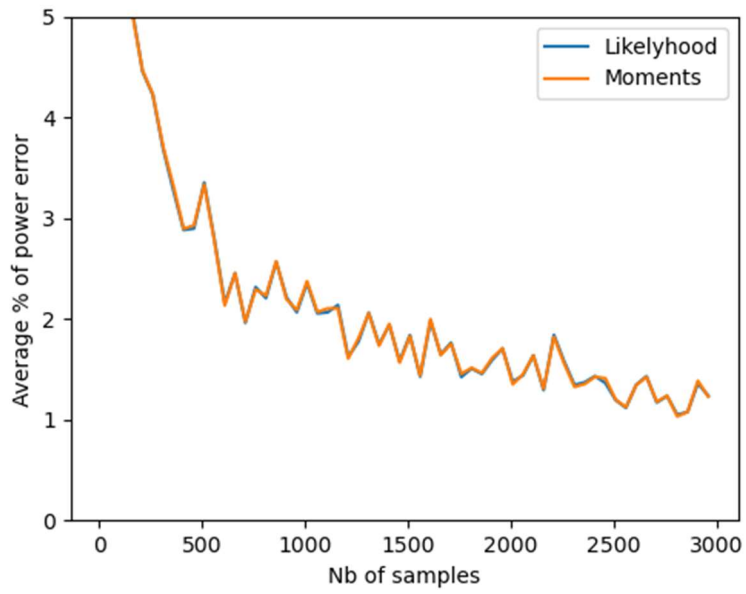
$$pdf(U) = \frac{k}{\lambda} \left(\frac{U}{\lambda}\right)^{k-1} e^{-(U/\lambda)^k} \quad \text{Eq. (2)}$$

where λ is a scale parameter in m s⁻¹ and k a dimensionless shape parameter. These parameters can be obtained by maximum likelihood, or by the method of the moments with the following formulas (Pavia and O'Brien, 1986):

$$k = (\sigma/\mu)^{-1.086} \quad \text{Eq. (3)}$$

$$\lambda = \frac{\mu}{\Gamma\left(\frac{1}{k}+1\right)} \quad \text{Eq. (4)}$$

where μ is the mean wind speed, σ the wind speed standard deviation, both in m s⁻¹, and Γ the Gamma function. The accuracy of these two methods was assessed with simulations. A random variable following a Weibull law with known parameters was generated and the equivalent wind power computed. For both methods, the results were compared with the wind power computed with the original parameters. Figure 6-3 shows the wind power mean absolute error in percentage as a function of the number of samples. With 500 samples, which is approximately the amount of available SAR data available in the areas of interest (~~see Figures 4 and 5~~), the accuracy of these methods is $\pm 2\%$. Both methods yield similar results, therefore the method of the moment, which is simpler and faster to run, was chosen.



275

Figure 63: Wind power Average-mean absolute wind power error in percentage as a function of the number of samples, using the two maximum likelihood to fit the wind Weibull pdf (orange curve), or the method of the moments (blue curve) estimation methods.

The main limitation of SAR ~~data-satellites~~ is their low temporal sampling (one passage every two days for Sentinel-1 in Europe). ~~One~~ One advantage of this limitation~~is, however, is~~ that it guarantees the statistical independence of the measurements~~-. Nevertheless, However,~~ the satellites are on a sun-synchronous orbit, which means that they pass always at the same times of the day, in the morning or in the evening. As a result, they cannot fully see the intra-diurnal variability of the wind.

Figure 74 shows the mean wind speed at 10 m as a function of the hour of the day for each Lidar. It can be seen that the wind diurnal cycle is close to a 24 h period sinusoid. Therefore, ~~Since the satellites possiblepass at two possible passage-times of the day are-separated by 12 h, according to the Nyquist-Shannon sampling theorem, they should be able to capture this is enough to capture the majority of the majority of the intra-day 24 h period-variability. In order to assess-verify this~~ this source of error, we simulated the satellites' passages over the Lidars by computing t-he mean wind speed and the wind power usingby computing the mean wind speed using only the Lidar measurements realized around 5 AM or 5 PM and compared it with the actual mean wind speedat the satellites' passage times. These values were compared to those obtained using all Lidar measurements at any time of day. For each Lidar, The-the error-differences was-were found to be below 1% and 2%, respectively, for the mean wind speed and the wind power. The same analysis was done with the wind power and the error ~~was found to be below 2%. Figure 7 shows the mean wind speed as a function of the hour of the day for each Lidar. It can be seen that the diurnal cycle is close to a sinusoid. Since the satellite passage times are separated by 12 h, this is enough to capture the majority of the 24 h period-variability. Therefore, this source of error is limited, and we conclude thatthe~~ intra-diurnal variability does not prevent the use of SAR data-and that this source of error is limited. However, this conclusion needs to be validated in geographical areas where thermic winds are stronger than in the North Sea.

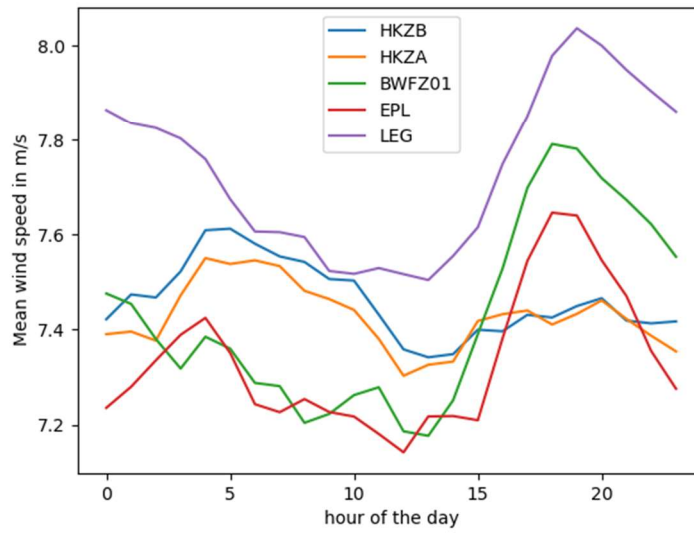
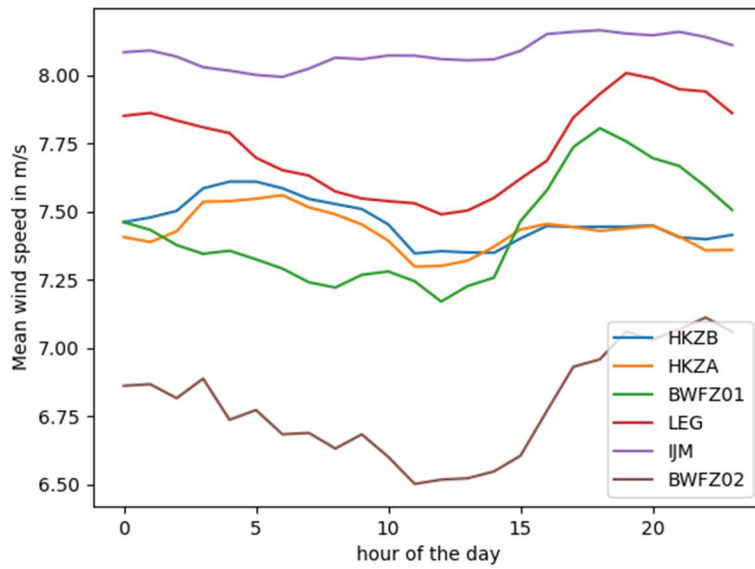


Figure 74: Intra-diurnal variability of the mean wind speed at 10 m for each Lidar. The time is given in UTC, which is close to the local time since the area of study Zone 1 and Zone 2 are located near Greenwich meridian.

305

3 Improvement of SAR surface wind estimates and extrapolation at hub height

3.1 Machine learning at surface level

SAR surface winds are obtained by inverting the backscatter over a given pixel with a Geophysical Model Function (GMF (see Section 2.3)). Originally, GMFs were designed to retrieve the wind from spaceborne scatterometers. ~~They were empirically designed using global numerical models as a reference.~~ However, SAR is a specific sensor and differences between the SAR and scatterometers backscatter in C-band may occur. In addition, ~~They GMFs were empirically designed using global numerical models as a reference, but, global numerical model outputs they~~ are not as reliable as in-situ data, especially in coastal areas. Moreover, GMFs may not fully capture the complex relation between the sea state and the wind, in particular because they assume a neutral atmosphere. As a result, SAR surface winds are typically biased when compared with in-situ buoys (see, e.g., de Montera et al., 2020). Therefore, it is necessary to improve the accuracy of ~~the~~ SAR wind speeds obtained with a GMF. This is particularly important because the wind power is related to the cube of the wind speed, and therefore very sensitive to wind speed estimation errors.

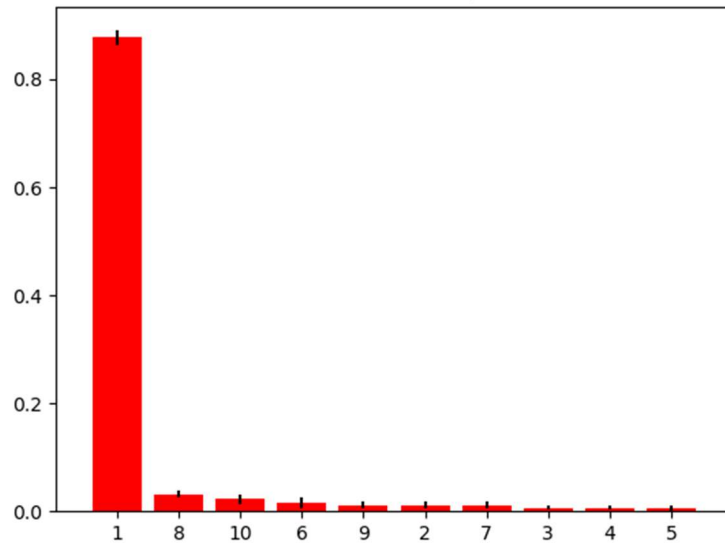
Given the complex relation between the sea state and the wind speed, and the number of factors able to influence it, machine learning was found to be an appropriate technique to improve the accuracy of SAR surface wind speeds and remove their biases.

~~We used a Two types of machine learning regressor were tested: the multi-layer perceptron and random forest. Random Forest algorithm (Breiman, 2001), which is known to perform well in regression tasks. It was implemented with the RandomForestRegressor function of Scikit-learn Python toolbox, and its architecture was chosen by using cross-validation. The default hyperparameters were found to be the bestmost appropriate ones, except the number of trees (set to 10240) and the maximum depth (set to 20). They were trained with the wind measured by the Lidars extrapolated to 10 m a.s.l. (the first Lidar level was extrapolated to this altitude with a power law, see Section 2.2). The algorithm was trained with the wind measured by the Lidars extrapolated to 10 m a.s.l. (the first Lidar level was extrapolated to this altitude with a power law, see Section 2.2). Combining all measurement sites, more than 1000 collocated data points between the Lidars and Sentinel-1 SAR could be found. The algorithm was trained with 50% of the data points chosen randomly chosen, and the rest of them were used as a test dataset.~~

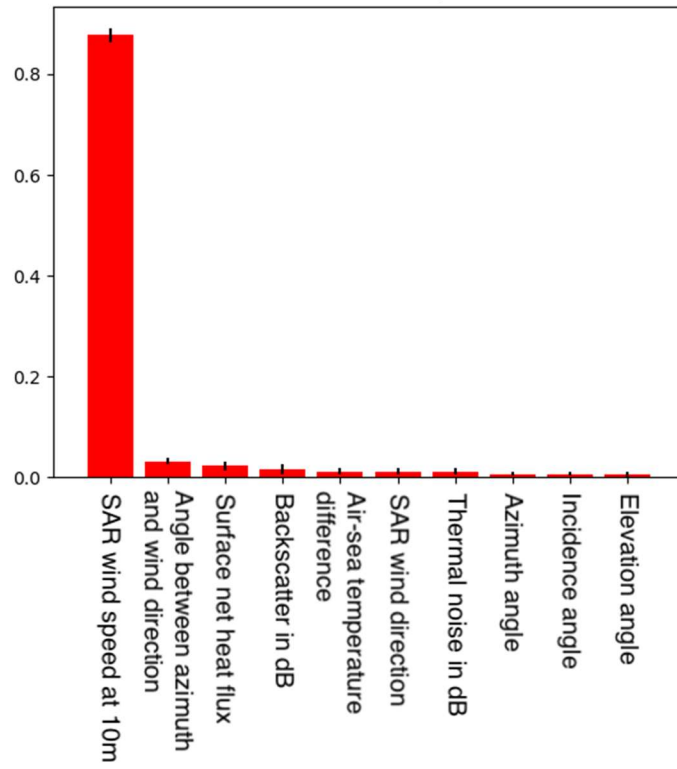
~~In order to select the input parameters, we made a list of interesting parameters and looked at for the ones having a relation with related to the level of absolute error differences between the SAR and the Lidars wind speeds. This was done visually by plotting scatterplots of scatter plots these parameters against the errors of the SAR compared to Lidar measurements and visual inspection were chosen by assessing their correlation with the error between the SAR and Lidar measurements.~~ The following parameters were ~~found to have such a correlation~~ selected: the SAR surface wind, the SAR wind direction, the azimuth angle (i.e., the angle between the North and the satellite track), the incidence angle (i.e., the angle between the radar illumination and the zenith of the target), the elevation angle (i.e., the angle between the radar illumination and the nadir of the satellite), the backscatter, the thermal noise of the instrument, and the difference between the azimuth angle and the wind

340 direction (an important parameter in the inversion of the backscatter). ~~Since the SAR surface winds are given assuming a~~
~~neutral atmosphere. The relative importance of these parameters after the training stage is shown in Figure 8. In order to take~~
the atmospheric stability ~~also needs to be taken~~ into account, ~~Therefore, the~~ air-sea temperature difference and ~~the~~ surface
heat flux were extracted from the high-resolution numerical model and ~~were~~ added as input parameters. ~~The relative~~
~~importance of these parameters was checked~~ measured after the training stage using the `feature_importances_` attribute of
345 ~~Scikit-learn Python toolbox (is shown in Figure 85). The relative importance of these parameters after the training stage is~~
~~shown in Figure 8.~~

Parameter relative importance



Parameter relative importance

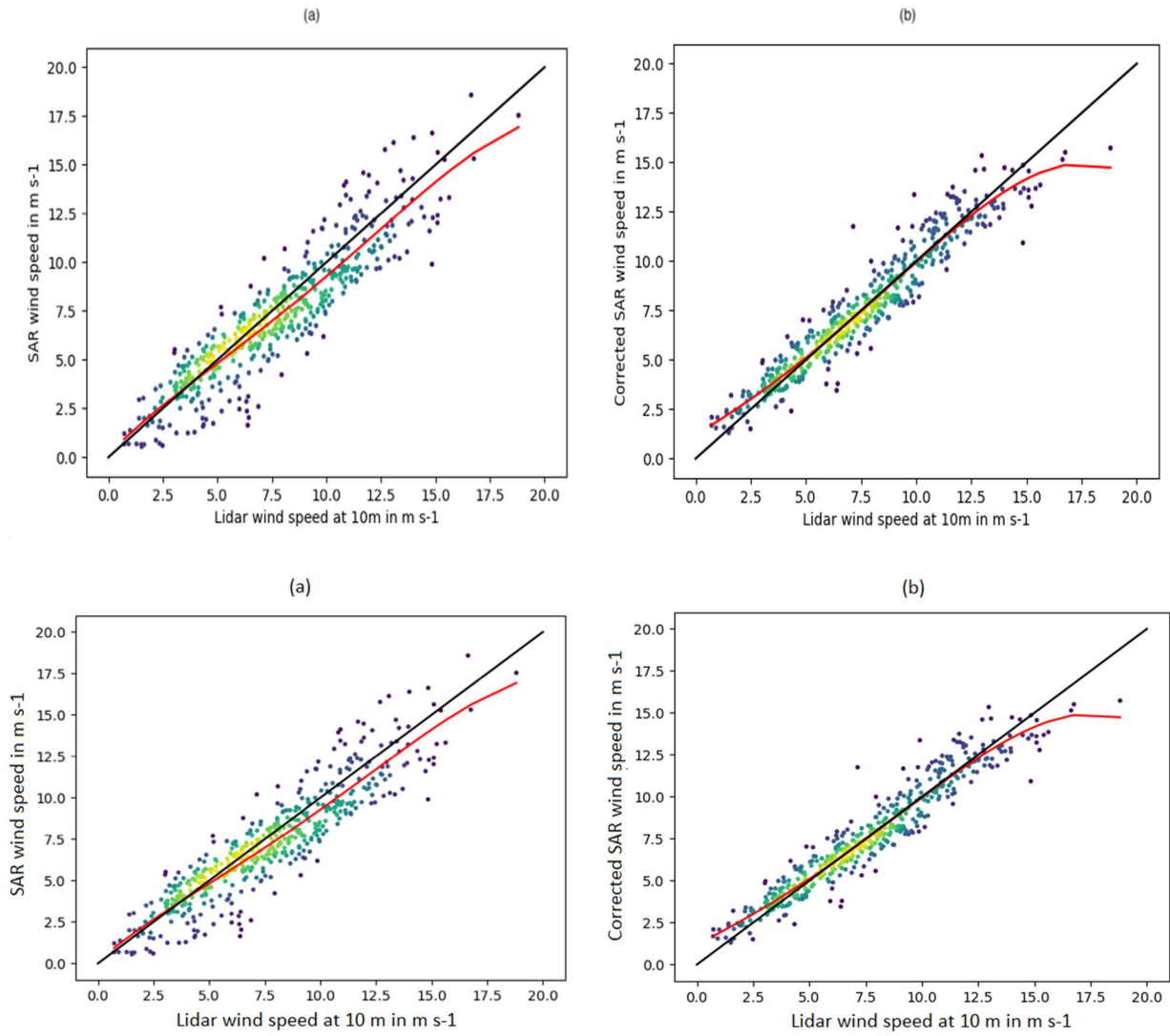


350 **Figure 85:** Relative importance of the input parameters used to correct the SAR surface wind at 10m with the ~~random~~ Random forest Forest algorithm (1—SAR wind speed, 2—SAR wind direction, 3—azimuth angle, 4—incidence angle, 5—elevation angle, 6—backscatter, 7—thermal noise, 8—difference between the azimuth angle and the wind direction, 9—air-sea temperature difference, 10—heat flux).

355 ~~The More than 1000 collocated data points between the Lidars and Sentinel-1 SAR could be found. The algorithm was trained with half of the data points, and the rest were used as a test dataset. Random forest was found to outperform neural networks in terms of performance and training time. It~~ Random Forest ~~algorithm is~~ was able to reduce the SAR wind speed bias from -0.42 m s⁻¹ to 0.02 m s⁻¹ and its ~~standard deviation~~ RMSE ~~standard deviation~~ from 1.41 m s⁻¹ to 0.98 m s⁻¹. Figures ~~9-6 and 10~~ shows the ~~scatterplots of errors between~~ the SAR wind speeds against and the Lidars measurements before and after applying machine learning. ~~The~~ It can be seen that the bias is indeed reduced, and that the cloud of points is thinner after machine learning. However, the resulting wind speeds are still biased at very low and very high wind speeds. These two ranges are more difficult to estimate because low wind speeds have little effect on the sea state, and because the relation between the sea state and the backscatter saturates at high wind speeds. A multi-expert algorithm using three ~~separated~~ different ~~random~~ Random forest Forest algorithms to process respectively low, middle and high wind speeds was tested. However, this approach did not improve the results ~~significantly~~.

360

365



370 **Figure 96: Scatterplots between the SAR and Lidar wind speeds at 10 m (a) before machine learning (a) and (b) after machine learning (b), with polynomial-fits (red-curves) using the test dataset. The colours represent the density of points. The black curve is the identity line and the red curve a fourth-degree polynomial fit illustrating the bias.**

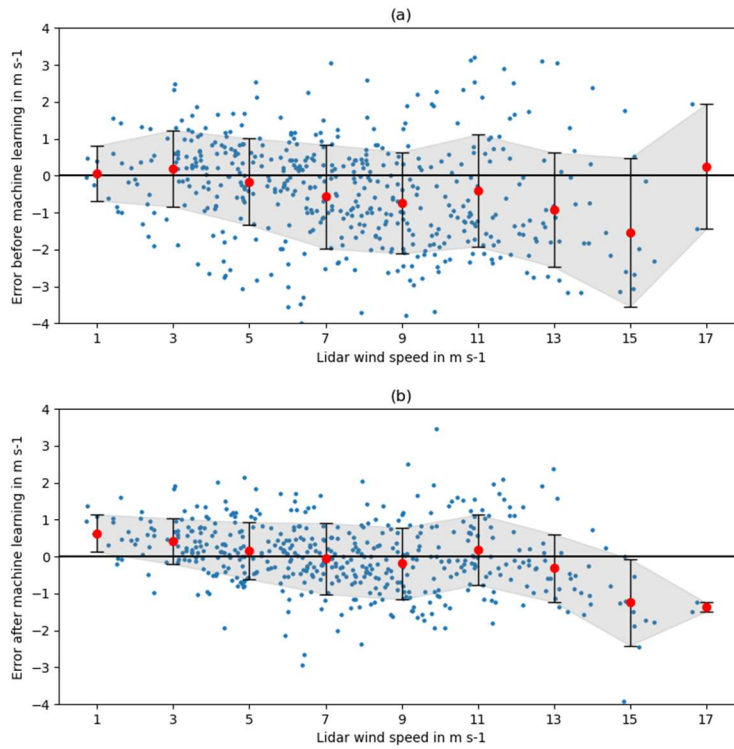


Figure 10: Errors between the SAR and the Lidars as a function of Lidar wind speed at 10 m (a) before machine learning (b) after machine learning.

375

3.2 Extrapolation at hub height

The extrapolation of surface wind speeds to higher altitudes is a challenging problem given the diversity of meteorological conditions and the variability of turbulence intensity in the boundary layer. Data analysis from offshore meteorological masts suggests that a simple power law could be sufficient to model the wind profile (Hsu et al., 1994). However, the analysis of our Lidar data shows that, above 40 m, this power law model is no longer accurate. This limitation has led some authors to use numerical models to improve the extrapolation to higher altitudes (Badger et al., 2016). The advantage of numerical models is that they provide information about atmospheric stability through parameters like surface temperature and surface heat flux. In Badger et al. (2016), these surface parameters were averaged and combined with the similarity theory of Monin-Obukhov to extrapolate wind Weibull parameters. However, to our knowledge, this method was validated with only one meteorological mast in the Baltic Sea and not higher than an altitude of 100 m. Moreover, Optis et al. (2021) found that using machine learning was more efficient than using a theoretical approach.

380

385

Therefore, we chose to extrapolate the instantaneous SAR wind speeds were also extrapolated with using a Random Forest algorithm. This algorithm machine learning using uses parameters extracted from the high-resolution WRF numerical model as additional input parameters. The most relevant parameters were found to be the air-sea temperature difference and the surface heat flux. In order to increase the accuracy and adapt to the current meteorological conditions, the model extrapolation ratio between the surface wind and the wind at hub height was also added. Comparing this ratio with the one found with the Lidar data showed that it is unbiased (for all Lidars, the bias was lower than 1%) and therefore suitable for extrapolating SAR winds. However, using comparisonss to the the Lidar measurements, it was found showed that the numerical model outputs were less accurate in the lower boundary layer, and that the mean wind speed was strongly biased below 40 m. Therefore, we decided to use the ratio between the wind speed at 40 m and higher altitudes, which was more accurate (for each Lidar, the ratio bias was lower than 1%). Comparing this ratio with the one found with the Lidar data showed that it is unbiased (for all Lidars, the bias was lower than 1%) and therefore suitable for extrapolating SAR winds. These parameters were used together with the corrected SAR wind speeds at 10 m as input to a the random Random forest Forest algorithm, which was and trained to learn the Lidar wind speed at 200m several altitude levels until 200 m, with 50% of the data points using the same training training and test dataset as in the previous section previously. The Here too, we used a Random Forest algorithm was also implemented with the RandomForestRegressor function of Scikit-learn Python toolbox. The most We used the default appropriate hyperparameters were found to be the default ones were found, except the number of trees (set to 83400) and, the maximum depth (set to 250 and the maximum number of features set to 'sqrt'). The relative importance of the parameters after the training phase is shown in Figure 7. The relative importance of the parameters is shown in Figure 11. Figure 12-8 shows the bias of the extrapolated SAR wind speeds against each Lidar in percentage as a function of the altitude. that The algorithm was successful in extrapolating SAR wind speeds because the these biases compared to Lidars is are stable with altitude and remains low and (comprised within $\pm 3\%$). At 200 m, The the SAR mean wind speed error bias at 200 m against all Lidars was was -0.04 m s^{-1} and its standard deviation RMSE standard deviation 1.69 m s^{-1} . Thus, this method provides an almost unbiased estimate of the wind speed at hub height. We also attempted to follow the same approach as Badger et al. (2016), in which the extrapolation is performed on wind statistics. However, the extrapolation of the wind power with the corresponding ratio provided by the numerical model was not as accurate as when the instantaneous winds were extrapolated first.

415

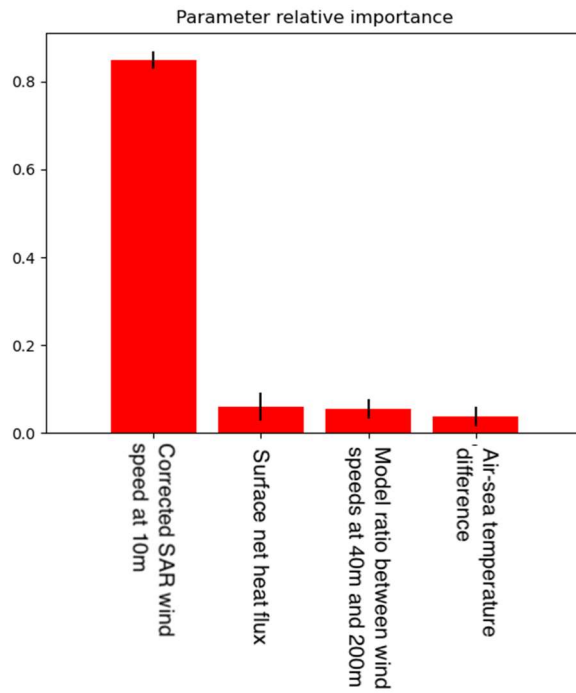
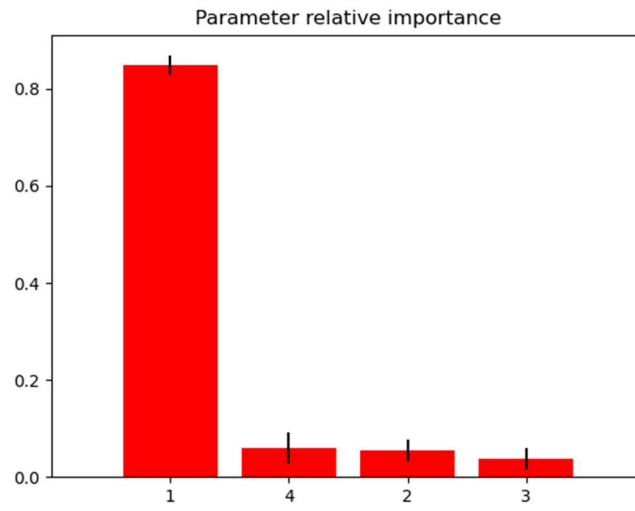


Figure 117: Relative importance of the input parameters used to extrapolate the SAR surface winds to 200 m. (1—Corrected SAR wind speed, 2—ratio of the numerical model wind speeds between 40 and 200 m, 3—air-sea temperature difference, 4—surface heat flux)

420

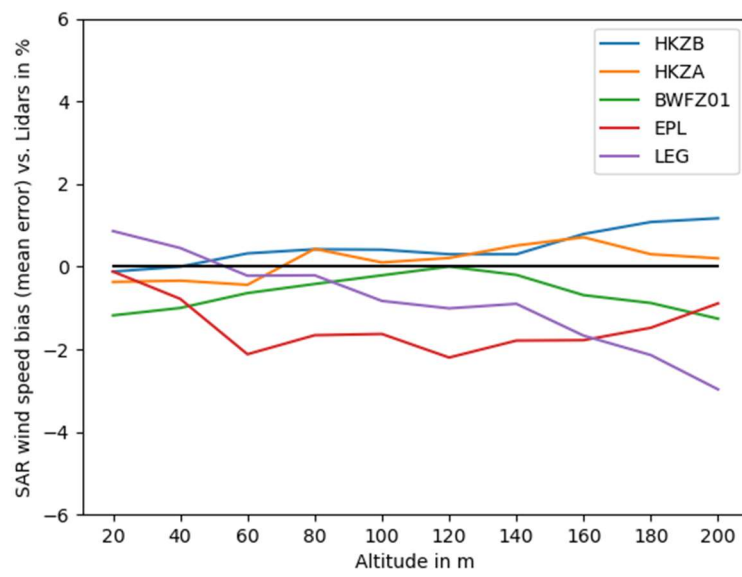
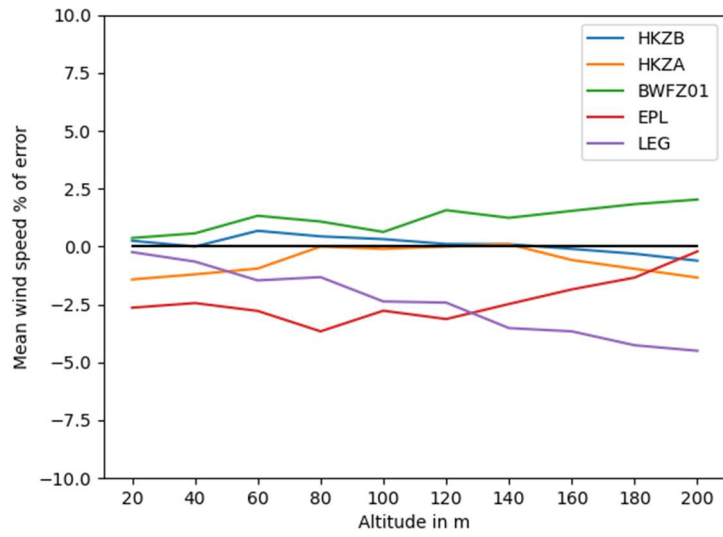


Figure 128: Bias of the extrapolated SAR wind speed against each Lidar at each Lidar location in percentage.

3.3 Machine learning at hub height with Lidar data

When profiling Lidars are available in the study area, the method accuracy can be improved by combining the correction of SAR surface winds and their extrapolation to higher altitudes into a single random Forest algorithm. In that case, the algorithm is trained directly at hub height with all the input parameters together. The relative importance of the input parameters after the training is shown in Figure 13. The results with the test dataset are shown in Figure 14. At 200m, the wind speed biases compared to each Lidars are within $\pm 2\%$. The total bias is 0.04 m s^{-1} and the standard deviation RMSE is 1.61 m s^{-1} . This result is better than the method presented in Section 3.2 using two separate steps. Therefore, this second method should be used if on-site profiling Lidars are available.

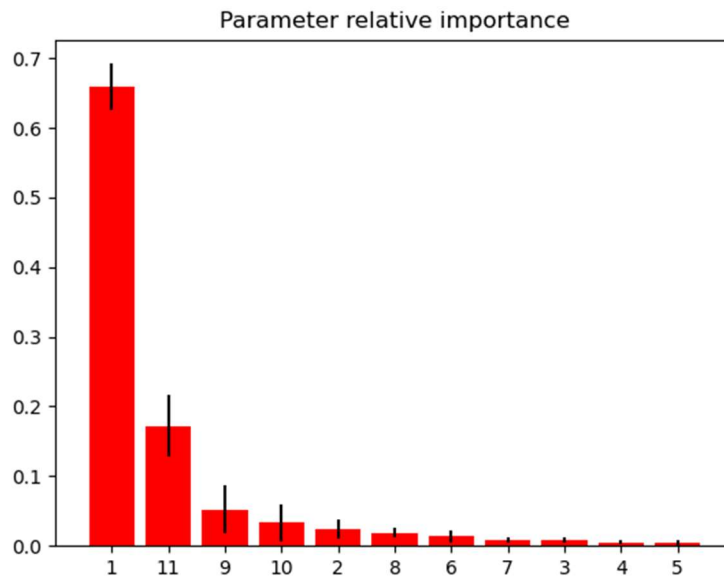


Figure 13: Relative importance of the input parameters used to correct and extrapolate the SAR wind speed at 200m (1— SAR wind speed, 2— SAR wind direction, 3— azimuth angle, 4— incidence angle, 5— elevation angle, 6— backscatter, 7— thermal noise, 8— difference between the azimuth angle and the wind direction, 9— ratio of the numerical model wind speeds between 40 and 200 m, 10— air sea temperature difference, 11— heat flux).

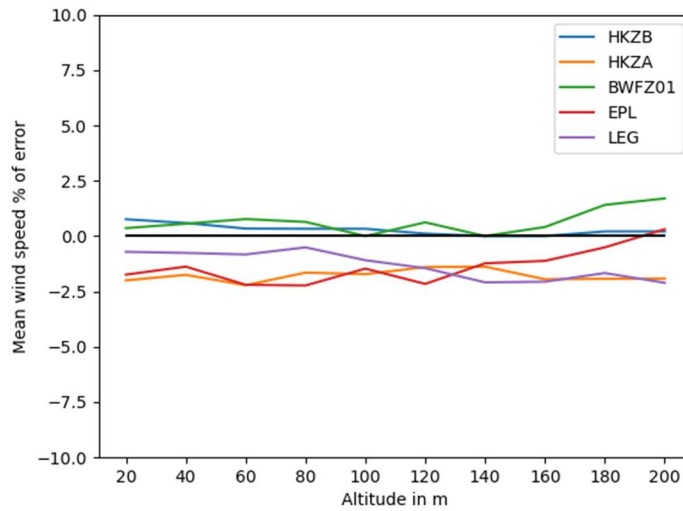


Figure 14: Bias of the extrapolated SAR wind speed at each Lidar location (algorithm trained directly at hub height).

4 Results

445 4.1 Correction of the standard deviation

As explained in Section 2.4, in order to estimate the extractible wind power, the Weibull parameters of the wind are needed. These parameters are directly linked to the first two moments of the wind speed distributionpdf, which are the mean wind speed and the wind speed standard deviation (see Eqs. 3 and 4). Therefore, an accurate estimation of these two moments alone is enough to guarantee a low error of the extractible wind power. The extrapolation methods presented above provide an unbiased estimation of the mean wind speed. However, the wind speed standard deviation was found to be biased and underestimated. This occurs because machine learning estimates the most probable expected value of the wind speed, which tends to reduce the variability of the wind speed: it squeezes its distribution because the errors are not reproduced. As a consequence, does not necessarily reproduce the original distribution shape of the data is not conserved. Its tails are lighter, and the standard deviation is underestimated. For example, at very low wind speeds, SAR sensors are often

450 unable to detect any effect on the sea state. Therefore, in this range, machine learning tends to produce the same most probable value, regardless of the SAR wind speed. The same happens at very high wind speeds, for which the instrument saturates. As a result, the distribution tails become lighter, which reduces the wind speed standard deviation. Figure 15-9 shows an example of the wind speed distribution obtained at 200 m after machine learning compared to the one obtained with Lidar HKZA. In that case, The error of the wind speed standard deviation bias was on average -6% and -9% respectively for the two-step

460 and single-step methods.

In order to compensate for this effect, we reintroduced artificially the original variability of the data. This was done by analysing the distribution of the SAR wind speed errors compared to Lidar measurements and adding a similar random variable to the SAR wind speed obtained after machine learning. The appropriate random variable was found to be a Gaussian with the standard deviation of the SAR wind speed errors. For each data point, at least five additional artificial datapoints needed to be created for the wind speed standard deviation to converge. After this bootstrap, the wind speed standard deviation error was 1.5% when considering all Lidars together in the test dataset. Thus, the result of this correction is an almost unbiased estimation of the wind speed standard deviation.

Figure 9 also shows the wind speed distribution provided by the high-resolution numerical model. In this case, the distribution was shifted to the left (Figure 15), which means that the numerical model underestimates the wind speed compared to Lidar measurements. This wind speed bias was found to be -4%. It was also corrected. Therefore, the opposite corrections were applied before computing the extractible power. By adding the opposite quantity to the model outputs in order to ensure a fair comparison with the numerical model, the same approach was applied to its outputs. In this case, the distribution was shifted to the left (Figure 15), which means that the model underestimates wind speed. This bias of -4% was also corrected.

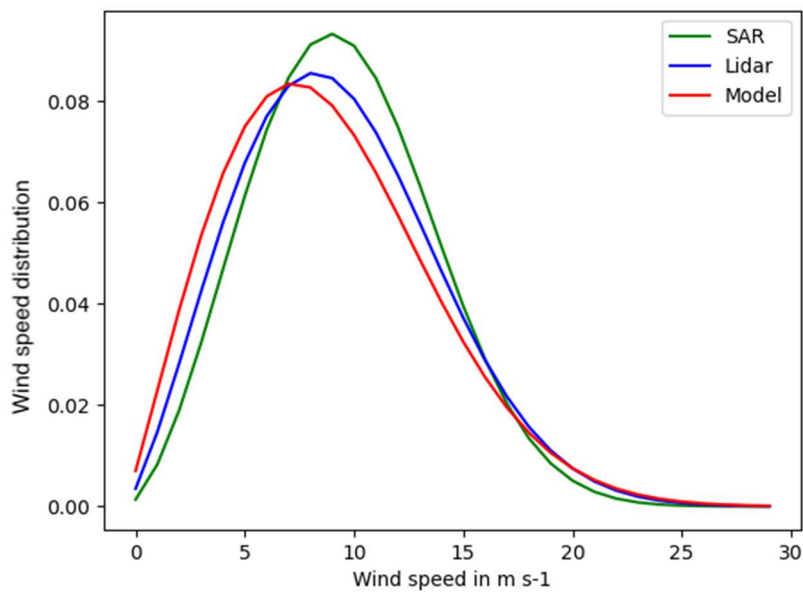


Figure 159: Wind speed distribution at 200m measured by Lidar HKZA compared to the ones obtained with SAR data combined with machine learning at hub height, and the numerical model at the same location.

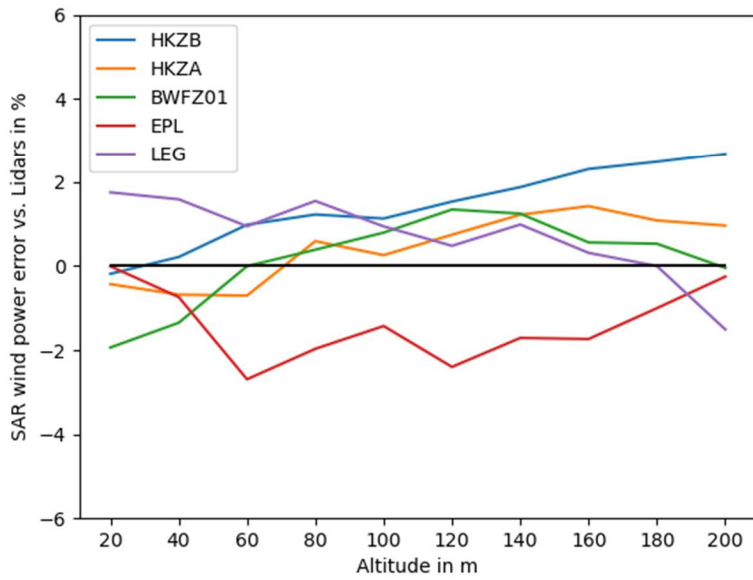
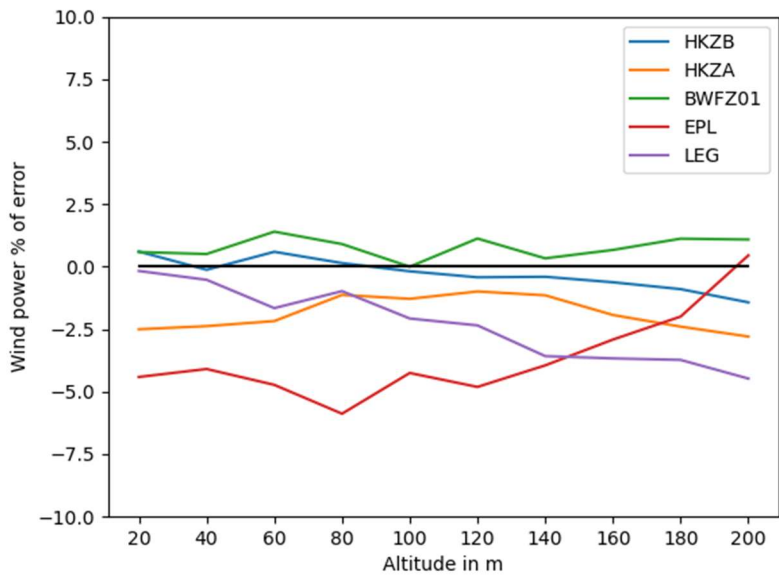
4.2 Extractible wind power at hub height

480 Once the wind speed ~~mean and~~ standard deviation had been corrected for ~~their~~ its biases, the estimation of the extractible power was done with the method presented in Section 2.4. The Weibull parameters were obtained with Eqs. 3 and 4, and then the wind power was obtained by multiplying the Weibull distribution (Eq. 2) by the typical 8-10 MW turbine power curve. Figures ~~16 and 17~~ 10, respectively, shows the bias of the wind power between the SAR and the Lidars in percentage. results for the two-step method and the single-step method using profiling Lidars. The method accuracy is $\pm 4\%$ ~~in the first case and $\pm 3\%$ in the second case.~~ When on-site profiling Lidars are available, the accuracy is close to the error bar of the wind power retrieval method (i.e., $\pm 2\%$, see Section 2.4). ~~When profiling Lidars are not available and the two steps method must be used, our result indicates that the loss of accuracy would be limited. However, this~~ Due to the short distances between the Lidars used in this study, such a validation could not be realized here. ~~this conclusion result~~ needs to be confirmed in another geographical locations than the North Sea. In areas where the machine learning algorithm trained in the North Sea would not be appropriate due to very different wind patterns, and where Lidar measurements are not available, a simpler method could be used. ~~where the correction of SAR surface winds could be performed with an algorithm trained with a different dataset such as metocean buoys, providing a higher number of collocated points, and where the extrapolation step would be validated with independent Lidar measurements. Due to the short distances between the Lidars used in this study, such a validation could not be realized here. However, w~~ We also tested another using extrapolation method without any machine learning by using directly ~~directly~~ the extrapolation ratio given by the high-resolution numerical model, without machine learning. In that case, the wind power error was comprised between $\pm 7\%$ for each Lidar, which is accurate enough to provide useful high-resolution mapsinsights about the coastal wind gradient. ~~.~~

485

490

495



500 **Figure 1610: Bias SAR wind power error in % compared to the one computed with Lidars measurements of the SAR-extractible power at each Lidar location, (two-step algorithm).**

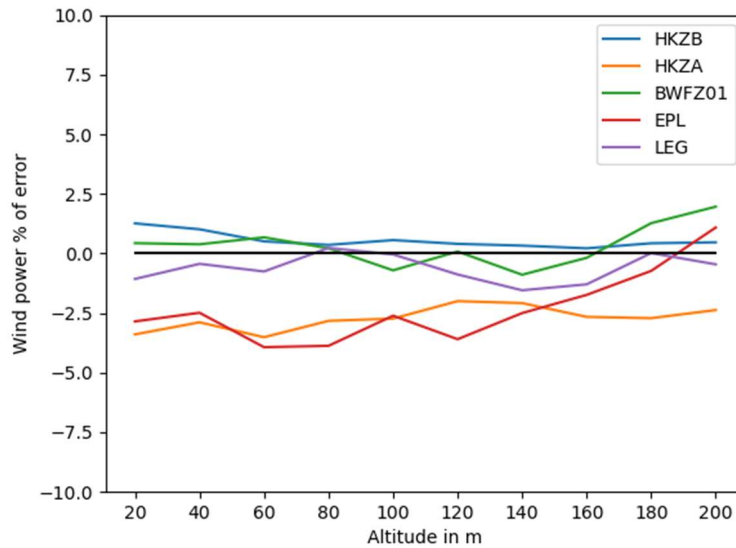
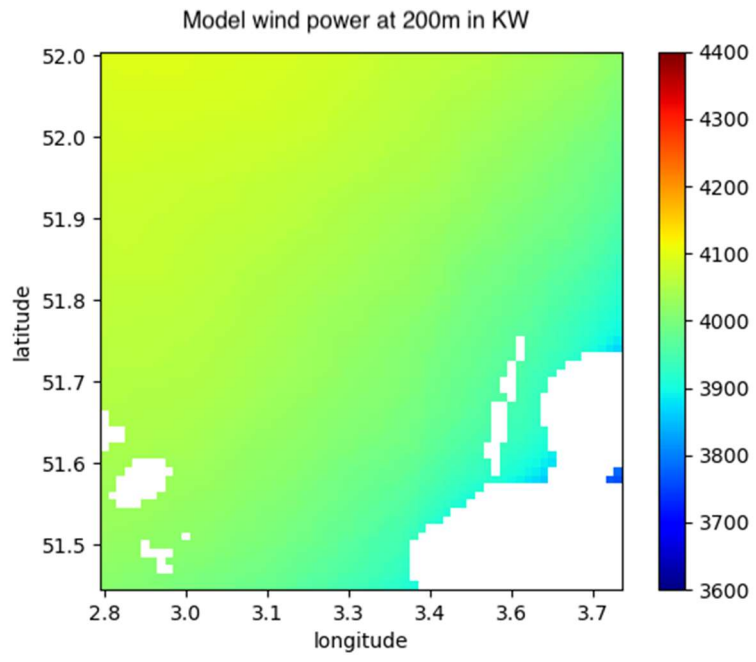


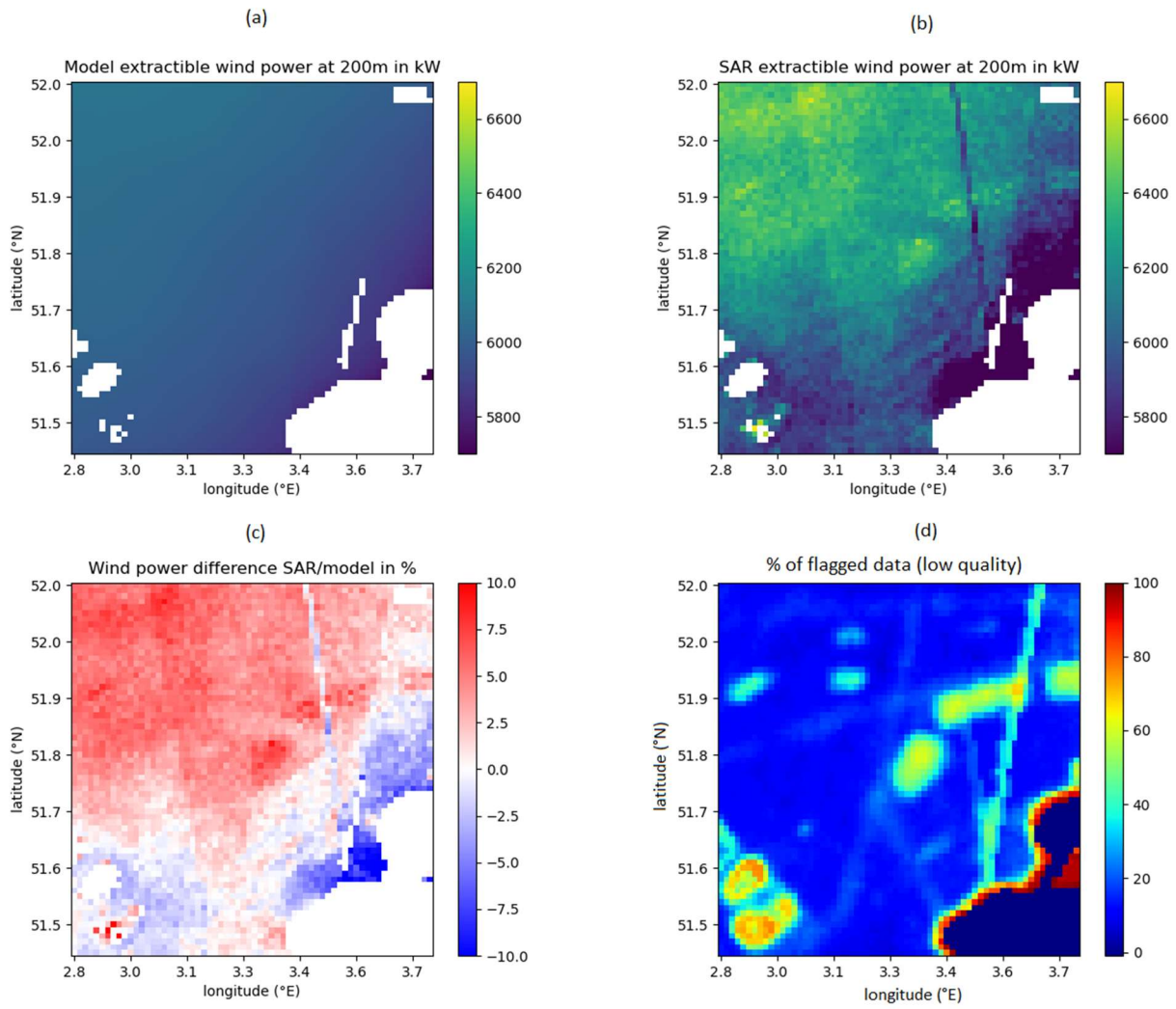
Figure 17: Bias of the SAR extractible power at each Lidar location (algorithm trained directly at hub height).

505 4.3 Wind power maps at hub height

Figures 18-11 and 19-12, respectively, show the extractible wind power maps at 200 m over Zone 1 and Zone 2 for the typical 10MW turbine. They present the wind power predicted by the numerical model, the wind power obtained with SAR data and machine learning, and the difference between these two in percentage. It can be seen that Figures 20 and 21 show the wind power obtained from SAR data for the same areas using the algorithm trained directly at hub height. Figures 22 and 23 show the difference in percentage between the maps obtained with the numerical model and the ones obtained with the SAR. The use of SAR data significantly increases the level of detail compared to the numerical model outputs. That correction difference can reach as much as 10% of the wind power between two sites separated by less than 20 km.

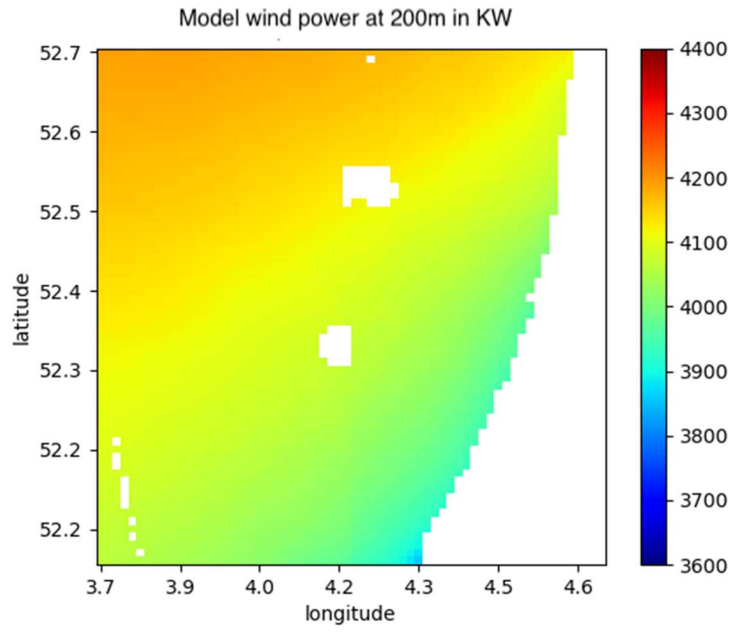
Some artefacts are still visible on the maps and need to be corrected in the future. For example, the swath edges can still be seen. Moreover, in some areas, the estimation was less reliable, mainly due to bright targets that could not be filtered. Some of these areas are linked to existing wind farms having a high density of turbines, while other areas had large numbers of stationary shipping vessels. The presence of these artefacts was measured by a Koch filter and a quality flag was created. Figures 24-11 and 25-12 also show the percentage of SAR data flagged as 'bad low quality', and therefore the areas where the assessment with SAR satellites is unreliable. In addition, in Zone 1, a series of three unrealistic 'waves' can be seen close to the coast. We could check that these patterns correspond to similar 'waves' of sand in the seabed. The bathymetry in these shallow waters seems to affect currents and, therefore, the SAR backscatter.

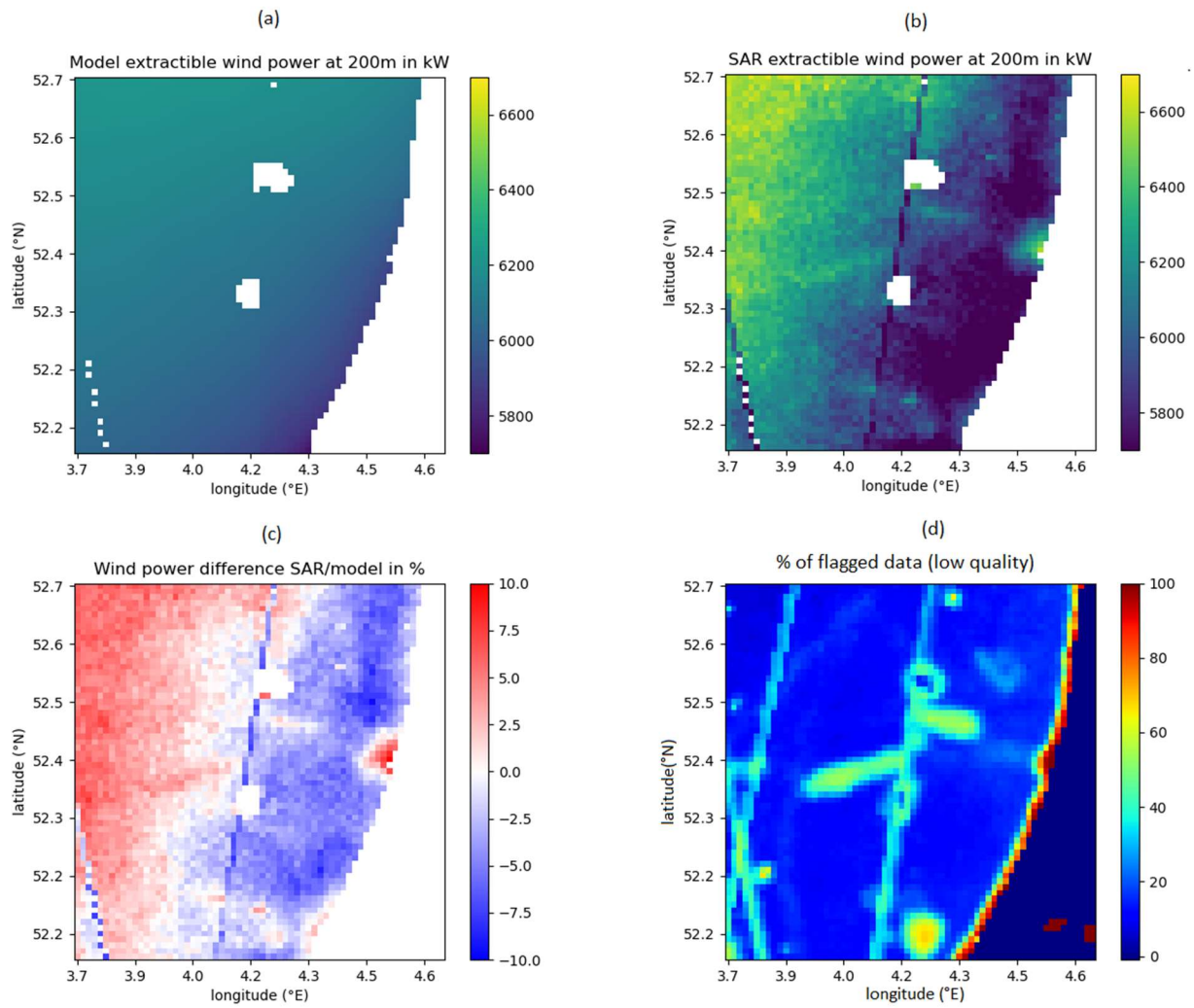




525

Figure 1811: Extractible wind power over Zone 1 in kW for a typical 10 MW turbine predicted by the numerical model (a) and SAR satellites (b), difference in percentage (c), and percentage of low-quality SAR data (d). Model-wind power at 200m for a typical 8 MW wind turbine over Zone 1.





530

Figure 1912: Extractible wind power over Zone 2 in kW for a typical 10 MW turbine predicted by the numerical model (a) and SAR satellites (b), difference in percentage (c), and percentage of low-quality SAR data (d).

Model wind power at 200m for a typical 8 MW wind turbine over Zone 2.

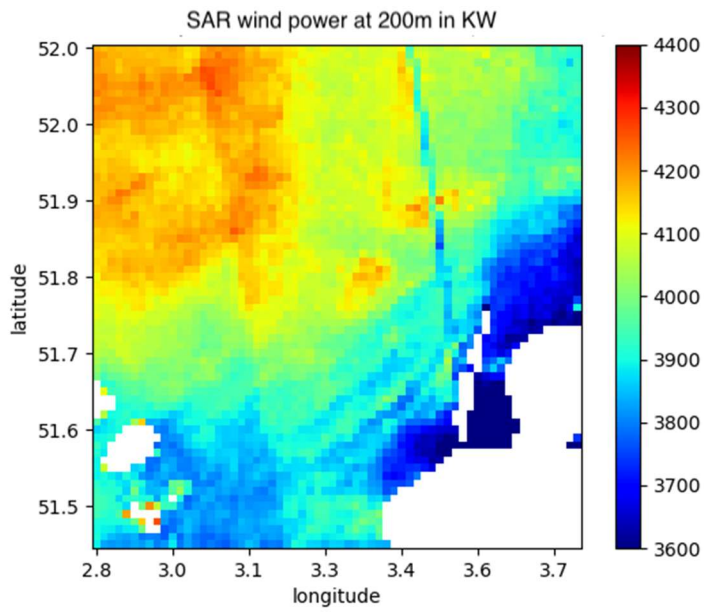
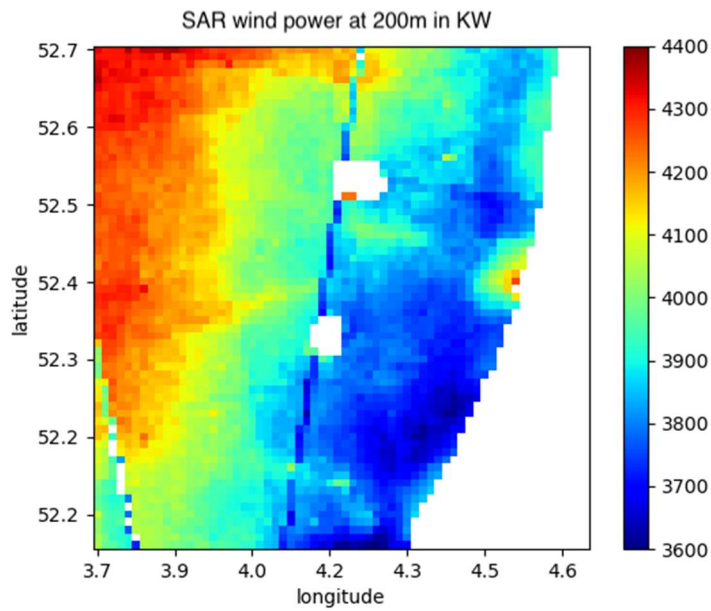


Figure 20: SAR wind power at 200m for a typical 8 MW wind turbine over Zone 1 (algorithm trained directly at hub height).



535 Figure 21: SAR wind power at 200m for a typical 8MW wind turbine over Zone 2 (algorithm trained directly at hub height).

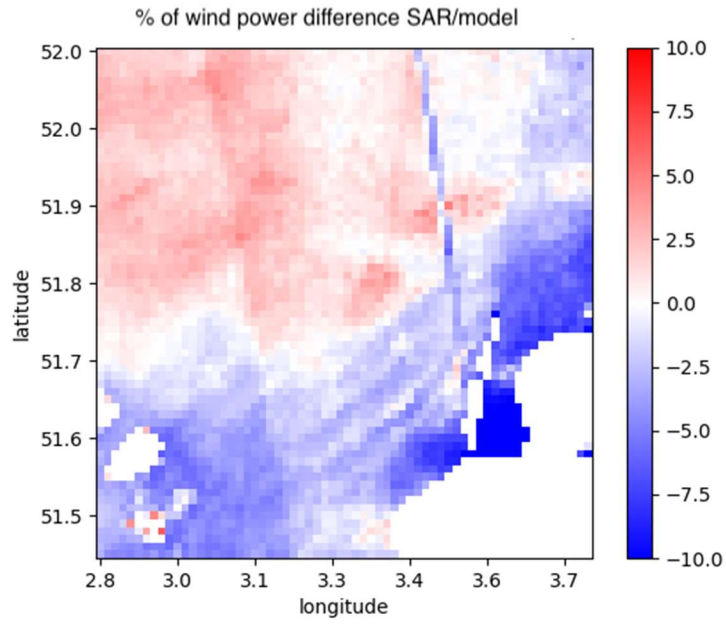


Figure 22: Percentage of difference between SAR wind power and the model wind power over Zone 1.

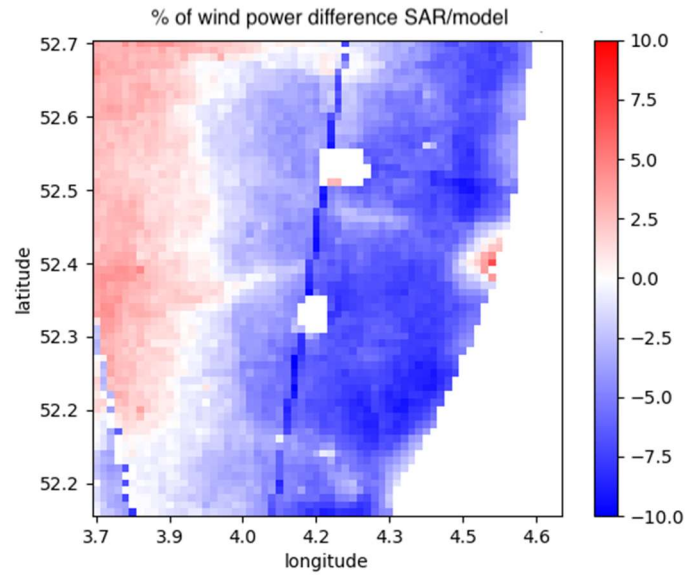


Figure 23: Percentage of difference between SAR wind power and the model wind power over Zone 2.

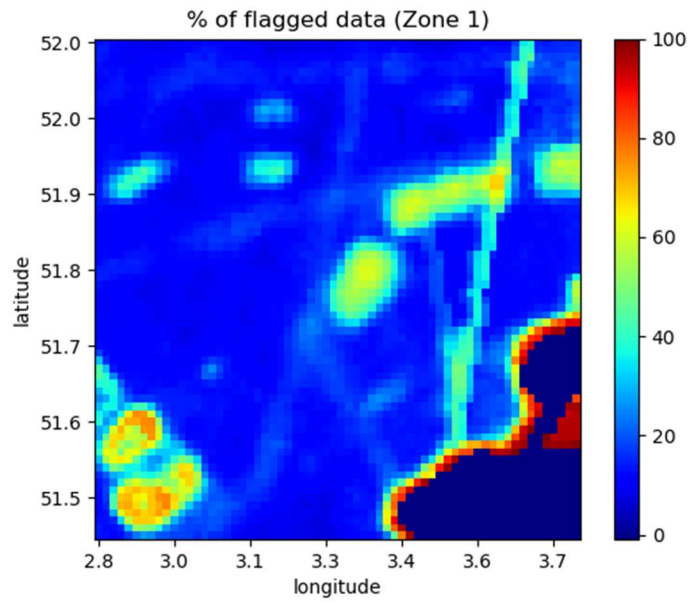
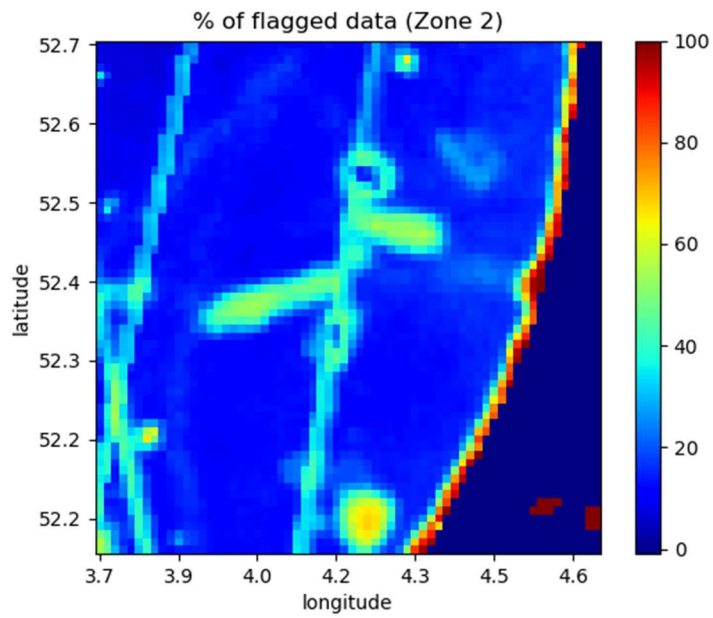


Figure 24: Percentage of data flagged as 'bad quality' over Zone 1.



545 Figure 25: Percentage of data flagged as 'bad quality' over Zone 2.

5 Conclusion

A new method for estimating the offshore extractible wind power at turbine hub height based on SAR data and machine learning has been presented. ~~If profiling Lidars are available, the machine learning algorithm can be trained directly at turbine hub height with geometrical parameters of the SAR sensor and parameters related to the atmospheric stability. If no Lidar is available,~~ The method ~~can be separated into~~ has two steps: first correcting SAR surfaces wind speeds with a machine learning algorithm fed with using geometrical parameters of the SAR sensor and meteorological parameters extracted from a high-resolution numerical model, surface wind measurements as a reference ~~and~~ then extrapolating these winds to higher altitudes with ~~a second~~ another machine learning algorithm. The method was tested in two areas off the Dutch coast using data from 5 Doppler wind Lidars installed on the sea surface. The ~~extractible~~ wind power maps were computed assuming a typical 8-10 MW turbine power curve. At 200m ~~above sea level~~ a.s.l., the accuracy of the method ~~in which the algorithm is trained directly at hub height~~ was 23% for both the wind speed and 3% for the wind power. ~~Regarding the two-step method, the accuracies were 3% and 4% respectively.~~ One must add the error due to intra-diurnal variability, which is not seen by the satellites. This source of error ~~which~~ was estimated to be less than 1% for mean wind speed and 2% for wind power ~~in these areas~~. Note that this additional uncertainty could be easily removed in the future by simulating the passages of SAR satellites using the high-resolution numerical model, and precisely estimating the effect of their time sampling. In the areas affected by the coastal gradient, the difference between the SAR wind power maps and the outputs of the numerical model can reach 10% over short distances of less than 20 km.

Compared to the maps provided by the numerical model, this method has the advantage of providing a much higher level of details. ~~In the areas affected by the coastal gradient, the difference between the SAR maps and the outputs of the numerical model can reach 10% of the wind power over short distances of less than 20 km.~~ Therefore, using SAR data combined with a high-resolution numerical model and processing them with machine learning can improve the assessment of the offshore wind resource. It can provide useful insights to optimize wind farm siting and risk management.

Further research should focus on removing some artefacts remaining on the SAR wind power maps, such as the swath edges, bright targets, and the effect of bathymetry. The method could also be improved by identifying other useful input parameters for machine learning, like the cross-polarization backscatter, which is more sensitive to strong winds. ~~One objective is also to improve the machine learning algorithm in order to obtain a better description of the Weibull distributions tails and avoid having to adjust them with a reference distribution.~~ Finally, the method needs to be generalized to other geographical areas ~~with independent~~ and trained with a larger training dataset that could combine in-situ measurements from Lidars and classical metocean buoys ~~measurements for assessing the wind speed accuracy at the sea surface and higher altitudes.~~

Author contribution

Louis de Montera designed the algorithm and wrote the paper. Henrick Berger processed the SAR raw data to create and created a Level 2 gridded wind product. Romain Husson provided his expertise on SAR satellite and wind measurement from space.

[Pascal Appelghem parametrized the WRF model and performed the runs. Laurent Guerlou and Mauricio Fragoso supervised the study, organised the funding, and ~~created~~gathered together the project team.](#)

[Competing interests](#)

[The authors declare that they have no conflict of interest.](#)

585 **Acknowledgments**

The authors would like to thank ESA [and the Dutch Ministry of Economic Affairs and Climate Policy](#) for providing [freely](#) Sentinel-1 data ~~and the Dutch Ministry of Economic Affairs and Climate Policy~~ for providing the Lidar data, [respectively](#). We would also like to thank Rémi Gandoin from C2WIND for checking the quality of the Lidar data ~~and his useful insights, and~~ Cynthia Johnson for correcting the spelling and improving the article style, [and two anonymous referees for their contributions](#).

590 This research was funded by the French Space Agency (Centre National d'Etudes Spatiales).

References

Ahsbahs, T., Badger, M., Karagali, I. and Guo Larsén, X.: Validation of Sentinel-1A SAR coastal wind speeds against scanning LiDAR. *Remote sensing*, 9(6), doi: 10.3390/rs906055, 2017.

595

Ahsbahs, T., MacLaurin, G., Draxl, C., Jackson, C., Monaldo, F. and Badger, M.: US East Coast synthetic aperture radar wind atlas for offshore wind energy. *Wind Energy Science*, 5, 1191-1210. doi: 10.5194/wes-5-1191-2020, 2020.

600 Badger, M., Peña, A., Hahmann, A. N., Mouche, A. A. and Hasager, C. B.: Extrapolating Satellite Winds to Turbine Operating Heights, *J. Applied Meteorology and Climatology*, 55(4), 975-991, doi: 10.1175/JAMC-D-15-0197.1, 2016.

Badger, M., Ahsbahs, T. T., Maule, P. and Karagali, I.: Inter-calibration of SAR data series for offshore wind resource assessment. *Remote Sensing of Environment*, 232, 111316, doi: 10.1016/j.rse.2019.111316, 2019.

605 Bentamy, A. and Croize-Fillon, D.: Spatial and temporal characteristics of wind and wind power off the coasts of Brittany. *Renewable energy*, 66, 670-679, doi: 10.1016/j.renene.2014.01.012, 2014.

[Breiman, L.: *Random Forests, Machine Learning*, 45\(1\), 5-32, 2001, doi: 10.1023/A:1010933404324](#)

610 Bodini, N. and Optis, M.: The importance of round-robin validation when assessing machine-learning-based vertical extrapolation of wind speeds. *Wind Energy Science*, 5(2), 489–501, doi:10.5194/wes-5-489-2020, 2020.

- 615 Chang, R., Zhu, R., Badger, M., Hasager, C.B., Zhou, R., Ye, D. and Zhang, X.: Applicability of synthetic aperture radar wind retrievals on offshore wind resources assessment in Hangzhou bay, China. *Energies*, 7, 3339-3354. doi: 10.3390/en7053339, 2014.
- Chang, R., Zhu, R., Badger, M., Hasager, C.B., Xing, X. and Jiang, Y.: Offshore wind resources assessment from multiple satellite data and WRF modeling over South China sea. *Remote Sensing*, 7, 467-487, doi: 10.3390/rs70100467, 2015.
- 620 Christiansen, M. B., Koch, W., Horstmann, J., Hasager, C. B. and Nielsen, M.: Wind resource assessment from C-band SAR. *Remote Sensing of Environment*, 105, 68-81, doi: 10.1016/j.rse.2006.06.005, 2006.
- De Zan, F. and Guarneri, A. M.: TOPSAR: Terrain Observation by Progressive Scans. *IEEE Trans. on Geoscience and Remote Sensing*, 44(9), 2352-2360, doi: 10.1109/TGRS.2006.873853, 2006.
- 625 [DTU Wind Energy. HAWC2 Model for the DTU 10-MW Reference Wind Turbine. 2017. https://www.hawc2.dk/Download/HAWC2-Model/DTU-10-MW-Reference-Wind-Turbine, last accessed September 2, 2021.](https://www.hawc2.dk/Download/HAWC2-Model/DTU-10-MW-Reference-Wind-Turbine)
- ECMWF. CMOD5.N: A C-band geophysical model function for equivalent neutral wind. Hersbach, H., 2008, 630 <https://www.ecmwf.int/en/elibrary/9873-cmod5n-c-band-geophysical-model-function-equivalent-neutral-wind>, last accessed 24 March 2021, 2008.
- Grachev, A. A. and Fairall, C. W.: Dependence of the Monin-Obukhov stability parameter on the bulk Richardson number over the ocean, *J. Applied Meteorology*, 36, 406-414, doi: 10.1175/1520-0450(1997)036<0406:DOTMOS>2.0.CO;2, 1996.
- 635 [Hahmann, A. N., Sīle, T., Witha, B., Davis, N. N., Dörenkämper, M., Ezber, Y., García-Bustamante, E., González-Rouco, J. F., Navarro, J., Olsen, B. T., & Söderberg, S.: The making of the New European Wind Atlas – Part 1: Model sensitivity. *Geoscientific Model Development*, 13\(10\), 5053-5078, doi: 10.5194/gmd-13-5053-2020, 2020.](https://doi.org/10.5194/gmd-13-5053-2020)
- 640 Hasager, C.B., Frank, H.P. and Furevik, B.R.: On offshore wind energy mapping using satellite SAR. *Canadian Journal of Remote Sensing*, 28(1), 80-89, doi: 10.5589/m02-008, 2002.
- Hasager, C.B., Nielsen, M., Astrup, P., Barthelmie, R., Dellwik, E., Jensen, N.O., Jørgensen, B.H., Pryor, S.C., Rathmann, O. 645 and Furevik, B.R.: Offshore wind resource estimation from satellite SAR wind field maps. *Wind energy*, 8, 403-419, doi: 10.1002/we.150, 2005.

- Hasager, C.B., Barthelmie, R.J., Christiansen, M.B., Nielsen, M. and Pryor, S.C.: Quantifying offshore wind resources from satellite wind maps: study area the North Sea. *Wind energy*, 9, 63-74. doi: 10.1002/we.190, 2006.
- 650
- Hasager, C.B., Badger, M., Peña, A., Larsén, X.G. and Bingöl, F.: SAR-Based Wind Resource Statistics in the Baltic Sea. *Remote Sensing*, 3, 117-144, doi: 10.3390/rs3010117, 2011.
- Hasager, C. B., Mouche, A., Badger, M., Bingöl, F., Karagali, I., Driesenaar, T., Stoffelen, A., Peña, A. and Longépé, N.:
655 Offshore wind climatology based on synergetic use of Envisat ASAR, ASCAT and QuikSCAT. *Remote sensing of environment*, 156, 247–263, doi: 10.1016/j.rse.2014.09.030, 2015.
- Hasager, C.B., Hahmann, A.N., Ahsbabs, T., Karagali, I., Sile, T., Badger, M. and Mann, J.: Europe's offshore winds assessed with synthetic aperture radar, ASCAT and WRF, *Wind Energy Science*, 5(1), 375-390, doi: 10.5194/wes-5-375-2020, 2020.
- 660
- Hersbach, H.: Comparison of C-band scatterometer CMOD5.N equivalent neutral winds with ECMWF. *J. Atmospheric Ocean Technology*, 27(4), 721-736, 2010, doi: 10.1175/2009JTECHO698.1, 2010.
- Hsu, S. A., Meindl, E. A. and Gilhousen, D. B.: Determining the power-law wind-profile exponent under near-neutral stability conditions at Sea, *Journal of Applied Meteorology and Climatology*, 33(6), 757-765, doi: 10.1175/1520-0450(1994)033<0757:DTPLWP>2.0.CO;2, 1994.
- 665
- Karagali, I., Peña, A., Badger, M. and Hasager, C. B.: Wind characteristics in the North and Baltic Seas from the QuikSCAT satellite. *Wind energy*, 17(1), 123-140. doi:10.1002/we.1565, 2014.
- 670
- KNMI. CMOD5.n—The CMOD5 GMF for neutral winds. Verhoef, A., Portabella, M., Stoffelen, A. and Hersbach, H., 2008, http://projects.knmi.nl/publications/fulltexts/cmod5_neutral_winds_1.0.pdf, last accessed 22 March 2021.
- Koch, W.: Directional Analysis of SAR Images Aiming at Wind Direction. *IEEE Transactions on Geoscience and Remote Sensing*, 42(4), 702–710, doi: 10.1109/TGRS.2003.818811, 2004.
- 675
- Mohandes, M. A. and Rehman, S.: Wind speed extrapolation using machine learning methods and LiDAR measurements. *IEEE Access*, 6, 77634-77642, doi: 10.1109/ACCESS.2018.2883677, 2018.

680 de Montera, L., Remmers, T., O'Connell, R. and Desmond, C.: Validation of Sentinel-1 offshore winds and average wind power estimation around Ireland, *Wind Energy Science*, 5(3), 1023-1036, doi: 10.5194/wes-5-1023-2020, 2020.

[NREL. Best Practices for the Validation of U.S. Offshore Wind Resource Models. Optis, M., Bodini, N., Debnath, M., and Doubrawa, P., 2020, https://www.nrel.gov/docs/fy21osti/78375.pdf, last accessed 24 August 2021.](https://www.nrel.gov/docs/fy21osti/78375.pdf)

685

Optis, M., Bodini, N., Debnath, M., and Doubrawa, P.: New methods to improve the vertical extrapolation of near-surface offshore wind speeds, *Wind Energ. Sci. Discuss.* [preprint], doi: 10.5194/wes-2021-5, in review, 2021.

Pavia, E. G. and O'Brien, J. J.: Weibull Statistics of Wind Speed over the Ocean. *Proceedings of the Royal Society of Mathematical, Physical and Engineering Sciences.*, 25(10), 1324-1332, doi: 10.1175/1520-0450(1986)025<1324:WSOWSO>2.0.CO;2, 1986.

690

Pimenta, F., Kempton, W. and Garvine, R.: Combining meteorological stations and satellite data to evaluate the offshore wind power resource of Southeastern Brazil. *Renewable energy*, 33(11), 2375-2387, doi: 10.1016/j.renene.2008.01.012, 2008.

695

Remmers, T., Cawkwell, F., Desmond, C., Murphy, J., and Politi, E.: The Potential of Advanced Scatterometer (ASCAT) 12.5 km Coastal Observations for Offshore Wind Farm Site Selection in Irish Waters. *Energies*, 12(2), 206, doi: 10.3390/en12020206, 2019.

700

Sánchez, R. F., Relvas, P., and Pires, H. O.: Comparisons of ocean scatterometer and anemometer winds off the southwestern Iberian Peninsula. *Continental shelf research*, 27(2), 155-175, doi: 10.1016/j.csr.2006.09.007, 2007.

705

[Skamarock, W. C., J. B. Klemp, J. Dudhia, D. O. Gill, Z. Liu, J. Berner, W. Wang, J. G. Powers, M. G. Duda, D. M. Barker, and X.-Y. Huang: A Description of the Advanced Research WRF Version 4. NCAR Tech. Note NCAR/TN-556+STR, 145 pp., doi:10.5065/1dfh-6p97, 2019.](https://www.ncl.ucar.edu/Technology/Documentation/2019/01/ncar_tn556str.pdf)

710

Türkan, Y. S., Yumurtacı Aydoğmuş, H. and Erdal, H.: The prediction of the wind speed at different heights by machine learning methods. *Inter. J. of Optimization and Control: Theories & Applications*, 6(2), 179–187. Doi: 10.11121/ijocta.01.2016.00315, 2016.

Vassallo, D., Raghavendra K., and Harindra J. S. F.: Decreasing wind speed extrapolation error via domain-specific feature extraction and selection. *Wind Energy Science*, 5(3), doi: 10.5194/wes-5-959-2020, 2020.

